Chinese Remainder Theorem-based Frequency Estimation for Undersampled Signals Without Multi-rate Sampling

Jiahui Cao[a,b], Zhibo Yang[a,b,*], Asoke K. Nandi[c]

[a] *National Key Lab of Aerospace Power System and Plasma Technology, Xi'an Jiaotong University, 710049, Xi'an, P.R. China*
[b] *School of Mechanical Engineering, Xi'an Jiaotong University, 710049, Xi'an, P.R. China*
[c] *Department of Electronic and Electrical Engineering, Brunel University of London, UB8 3PH Uxbridge, U.K.*

Abstract

Frequency estimation of undersampled waveforms has received considerable attention in communications, instrumentation, and measurement fields. Chinese remainder theorem (CRT)-based reconstruction is a prevalent frequency estimation method. However, the existing CRT-based methods heavily rely on multi-rate sampling and face challenges in handling real-valued undersampled waveforms and multi-frequency scenarios due to inherent ambiguities. To overcome these limitations, we propose a novel CRT-based frequency estimation method that generates aliasing information through the phase change caused by delay and estimates frequencies by solving the congruence equations constructed using the aliasing findings. The proposed method requires only a specially designed periodic nonuniform sampling of order 2, which avoids multi-rate sampling and has a simpler hardware implementation. Owing to the clear correspondence between the multiple frequencies and their aliasing frequencies, the proposed method can be applied to multi-frequency estimations. Furthermore, the proposed method is extended to real-valued waveforms by incorporating grouping operations and frequency estimation sifting. In summary, this study overcomes the main limitations of CRT in frequency estimation of undersampled waveforms and shows superior applicability to real-valued signals and multi-frequency cases, which may lead to a renaissance of CRT in undersampling signal processing.

Keywords: Chinese remainder theorem, Delay coprime sampling, Grouping and sifting operation, Complex-valued and real-valued undersampled waveforms, Frequency estimation.

1. Introduction

Frequency estimation of sinusoidal signals from finite noisy samples is a fundamental problem in digital signal processing which has diverse applications [1–4]. Numerous frequency estimation methods have been proposed in recent decades, such as autoregressive spectral analysis [5], Prony's method [6], maximum likelihood [7, 8], and subspace method [9]. In these methods, signals are typically sampled at rates higher than the Nyquist rate. However, as the signal frequency increases, the Nyquist rate becomes more difficult to reach due to hardware or cost limitations in some applications [10, 11] and only undersampled waveforms are obtained.

*Corresponding author
Email addresses: caojiahui@stu.xjtu.edu.cn (Jiahui Cao), phdapple@mail.xjtu.edu.cn (Zhibo Yang), Asoke.Nandi@brunel.ac.uk (Asoke K. Nandi)

Consequently, frequency estimation of undersampled waveforms is drawing considerable attention, especially in communications, instrumentation, and measurements [12–15].

To enable undersampling beyond the generic restriction stated in the Shannon-Nyquist sampling theorem [16, 17], there is a main direction: making proper assumptions on the signal model. CRT-based reconstruction, short for CRT method, is an efficient deterministic method that makes a complex-valued sinusoid waveform assumption on the signal. CRT method is based on discrete Fourier transform (DFT) spectrum. It relies on multi-rate sampling and uses the DFT spectra of the collected samples at each uniform sampling rate to detect the aliasing frequency. Then the true frequency is estimated from these aliasing frequencies using CRT-based algorithms [18]. Conventional CRT aims to reconstruct a single integer from congruence equations with coprime moduli and error-free remainders, and is sensitive to remainder errors. A small remainder error may result in an unacceptable error in reconstruction. Conventional CRT faces three challenges:

1) In frequency estimation, moduli and remainders are sampling rates and the corresponding aliasing frequencies, which are usually not integers. Furthermore, even if the sampling rates are integer, they may not be coprime. Thus, CRT method is required to be generalized.

2) Remainder errors are inevitable in practice; thus, CRT method is required to be robust to errors or noises.

3) Considering that a signal usually contains more than one frequency in practice, CRT method is required to be able to reconstruct multiple frequencies.

The above three challenges/requirements encouraged the development of CRT method in the past two decades. Specifically, the milestones in the development of CRT can be concluded as the following.

To overcome the sensitivity to remainder errors, some redundancy is introduced by adding a common factor to moduli. This is the prototype of robust CRT (RCRT) pioneered by Xia [19]. For single frequency estimation, the search-based and maximum likelihood estimation-based RCRT were successively proposed in [20, 21] and [22]. In 2010, closed-form RCRT (CR-CRT) was first proposed by Wang and Xia [18], which can robustly estimate frequency when the remainder error is less than a quarter of the common factor of moduli. Owing to its closed-form, CR-CRT has significantly lower computational complexity than previous RCRTs. Furthermore, CR-CRT extends the applicability of this research beyond integers to real numbers. Following CR-CRT, a generalized version called multistage RCRT was proposed in [23], where moduli may not share the same common divisor. In multistage RCRT, partial moduli are selected in each step to improve the robustness against residual error. As for multiple frequencies estimation, existing works primarily focused on the robust reconstruction of two frequencies with erroneous remainders [24]. Although RCRT methods for multi-frequency reconstruction have been developed [25–27], their computational complexity may be unacceptable due to the ambiguity between multiple frequencies and their aliasing frequencies. In addition, extending RCRT to real-valued waveforms is another challenge. Due to the presence of negative frequency, there exists ambiguity between the aliasing frequency and remainder in the real-valued waveforms [28].

Motivations: In a nutshell, the CRT-based methods and its variants have three main limitations. First, they rely on multi-rate sampling and are unsuitable for simpler sampling patterns, resulting in high hardware

cost. Second, they are not efficient for multi-frequency estimation due to the ambiguity between multiple frequencies and their aliasing frequencies. Finally, they can barely handle real-valued waveforms, which severely limits their practicality. This study aims to develop a CRT-based method to address these limitations.

Contributions: In this study, we propose a novel CRT-based frequency estimation method that reduces the required sampling rate and simplifies hardware configurations. More importantly, the proposed method can be applied to real-valued waveforms and multi-frequency estimation, which greatly improves the practicality of CRT. Our main contributions are summarized as follows.

- We propose a minimal periodic nonuniform sampling (PNS), termed delay coprime sampling (DCS), and a corresponding algorithm, termed active aliasing time delay estimation (AATDE), to mine aliasing information from sub-Nyquist samples. This strategy avoids multi-rate sampling and generates aliasing information via data rearrangement.
- Using the aliasing findings, we develop a frequency reconstruction algorithm based on CRT for complex-valued waveforms and give the error tolerance bound. Furthermore, the frequency reconstruction algorithm can be extended to real-valued waveforms by introducing grouping operations and frequency estimation sifting.
- Owing to the clear correspondence between the multiple frequencies and their aliasing frequencies in AATDE, the proposed method can simplify the multi-frequency estimation problem to multiple independent single-frequency estimations, which greatly improves computational efficiency.

2. Preliminaries

2.1. Signal and aliasing models

We first consider a complex waveform with K components

$$x(t) = \sum\nolimits_{k=1}^{K} A_k e^{j(2\pi f_k t + \varphi_k)} + w(t), \tag{1}$$

where A_k, f_k, and φ_k respectively denote the amplitude, frequency, and phase of the kth component. $w(t)$ is the additive noise. j is imaginary unit, $j = \sqrt{-1}$.

Assume that $x(t)$ is sampled at rate f_s. Then, by Poisson's summation formula [29], we have

$$\boldsymbol{X}(f) = \sum_{n=-\infty}^{+\infty} x[n] e^{-j2\pi f n} = \frac{1}{T_s} \sum_{k=-\infty}^{+\infty} \tilde{\boldsymbol{X}}(f + k f_s), \tag{2}$$

where $x[n]$ is the discrete signal, $x[n] = x(n/f_s)$, and $T_s = 1/f_s$. $\boldsymbol{X}(f)$ denotes the discrete time Fourier transform (DTFT) of $x[n]$, and $\tilde{\boldsymbol{X}}(f)$ denotes the true spectrum of $x(t)$.

Eq. (2) indicates that $\boldsymbol{X}(f)$ is the periodic extension of $\tilde{\boldsymbol{X}}(f)$. Assuming f_s is less than the Nyquist rate, $\boldsymbol{X}(f)$ is aliased as shown in Fig. 1 in which a single frequency signal is considered for simplicity. Let f_t be the true frequency in $x(t)$, i.e., $\mathrm{supp}(\tilde{\boldsymbol{X}}(f)) = \{f_t\}$ where $\mathrm{supp}(\cdot)$ denotes the support of a function. Let $\tilde{\boldsymbol{X}}(f_t)$ be the Fourier coefficient at f_t. As expressed in (2), $\boldsymbol{X}(f)$ contains a series of frequencies, which are caused by

the periodic extension of f_t. In practice, we typically calculate the DFT spectrum, which is a section of $\boldsymbol{X}(f)$ in $[0, f_s)$. For complex-valued signals, the periodic extension result of f_t in DFT spectrum is referred to as the aliasing frequency f_a. Remarkably, $\boldsymbol{X}(f_a) = \tilde{\boldsymbol{X}}(f_t)$[1].

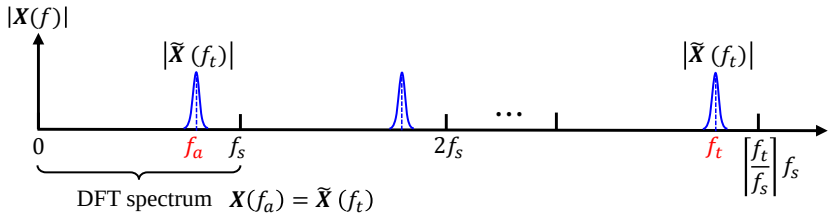

Figure 1: DTFT and DFT spectra of a sub-Nyquist complex-valued signal.

If the signal is real-valued, its DTFT spectrum has additional negative duplicates. If $x(t)$ is a real waveform, $\tilde{\boldsymbol{X}}(f)$ contains two opposite frequencies f_t and $-f_t$, and their Fourier coefficients are conjugate, i.e., $\tilde{\boldsymbol{X}}^*(f_t) = \tilde{\boldsymbol{X}}(-f_t)$. By (2), $\boldsymbol{X}(f)$ contains a series of frequencies caused by the periodic extension of f_t and $-f_t$, which are marked in blue and red lines, respectively (Fig. 2). For real-valued signals, there are two frequencies in DFT spectrum which are periodic extension results of f_t and $-f_t$. For real-valued signals, the periodic extension result of f_t or $-f_t$ in the left half of the DFT spectrum is referred to as aliasing frequency f_a. Remarkably, we only know that f_a is the periodic extension result of either f_t or $-f_t$, i.e., f_a is the modulus of either f_t or $-f_t$ with respect to f_s, but the precise correspondence is unknown. Therefore, there exist two possible relations between $\boldsymbol{X}(f_a)$ and $\tilde{\boldsymbol{X}}(f_t)$, as follows

Case 1: $\mathrm{mod}(f_t, f_s) \in [0, f_s/2)$. In this case, f_a is the modulus of f_t with respect to f_s; thus, $\boldsymbol{X}(f_a) = \tilde{\boldsymbol{X}}(f_t)$, as shown in Fig. 2(a).

Case 2: $\mathrm{mod}(f_t, f_s) \in [f_{s/2}, f_s)$. In this case, f_a is the modulus of $-f_t$ with respect to f_s; thus, $\boldsymbol{X}(f_a) = \tilde{\boldsymbol{X}}^*(f_t)$, as shown in Fig. 2(b).

The above observations clearly indicate the relation between the Fourier coefficients at true and aliasing frequencies, on which our following analysis will heavily rely.

2.2. Chinese remainder theorem

CRT states that a positive integer can be reconstructed from its remainders modulo a series of integer moduli, which has many applications. Specifically, it is formally given in

Chinese Remainder Theorem [30]: *let B be the positive integer to be reconstructed and let M_i, $1 \leqslant i \leqslant S$, be S pairwise coprime integers as moduli,*

$$\mathrm{mod}(B, M_i) = r_i \text{ or } B = n_i M_i + r_i \tag{3}$$

where r_i denotes the remainder of B modulo M_i, and n_i is an unknown integer (called folding integer). Then, the target integer can be uniquely reconstructed if

$$0 \leqslant B < \mathrm{lcm}\{M_1, M_2, \cdots, M_S\} \tag{4}$$

[1]The constant item T_s^{-1} is omitted here for brevity

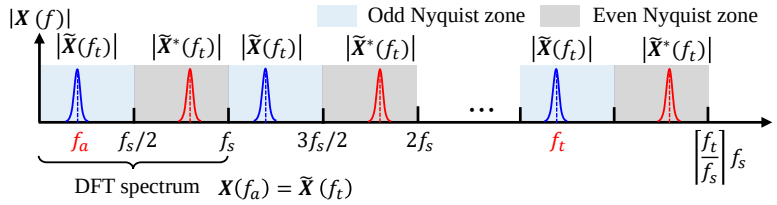

(a)

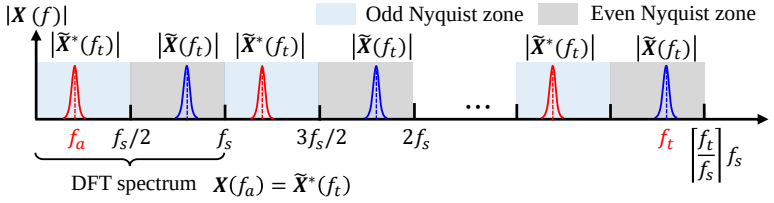

(b)

Figure 2: DTFT and DFT spectra of a sub-Nyquist real-valued signal: (a) case 1 and (b) case 2. Nyquist zones are regions of the spectrum that are divided into uniform intervals of $f_s/2$. Each zone contains a copy of the desired signal's spectrum or a mirror image of it. Here, the Nyquist zones $[\frac{(n-1)f_s}{2}, \frac{nf_s}{2})$ for $n = 1, 3, 5, \cdots$ and $n = 2, 4, 6, \cdots$ are referred to as odd and even Nyquist zones, respectively.

where $\mathrm{lcm}\{\cdot\}$ *denotes the least common multiple.*

Classical CRT is not robust against remainder errors. To overcome remainder errors, a CR-CRT algorithm [18] has been proposed for the reconstruction, which can accurately determine n_i and lead to a robust reconstruction if

$$|\hat{r}_i - r_i| \leqslant \gcd\{M_1, M_2, \cdots, M_S\}/4 = 1/4, \tag{5}$$

for each $1 \leqslant i \leqslant S$, where $\hat{r}_i$ denotes the erroneous remainders. $\gcd\{\cdot\}$ denotes the greatest common divisor.

CRT provides theoretical support for frequency estimation of sub-Nyquist signals. A complex signal $x(t) = e^{j2\pi f_t t}$ is sampled uniformly at the rate f_s, where $f_s < f_t$ and DFT is applied to the discrete samples. It is well known that undersampling will result in a spectrum aliasing, as depicted in Fig. 1: the location of the spectrum peak is $\mathrm{mod}(f_t, f_s)$ and is denoted by f_a. Therefore, if multi-rate sampling is achievable, we can construct congruence equations based on the aliasing results obtained from samples with different rates and estimate the true frequency by solving the equations. Coprime sampling (CS) is an efficient multi-rate sampling widely used in the existing CRT-based frequency identification methods. However, CRT-based methods encounter three main challenges in practice. 1) One is the additional hardware overhead due to multi-rate sampling. 2) Another is the ambiguity between the aliasing frequency and remainder in real-valued waveforms[2]. 3) The third challenge is the correspondence ambiguity between the true frequencies and their aliasing results in multi-frequency cases[3]. In the following, we propose a new CRT-based frequency estimation method that does not require multi-rate sampling and eliminates the above two ambiguities.

[2]For a real-valued waveform, f_a is equal to either $\mathrm{mod}(f_t, f_s)$ or $f_s - \mathrm{mod}(f_t, f_s)$, but the exact correspondence is unknown.

[3]For a complexed valued multi-frequency signal with $\{f_k\}_{k=1}^K$, coprime sampling with $\{f_{si}\}_{i=1}^S$ and DFT can only obtain the aliasing frequency sets $\mathbb{S}_1, \cdots, \mathbb{S}_S$, where $\mathbb{S}_i = \{\mathrm{mod}(f_1, f_{si}), \cdots, \mathrm{mod}(f_K, f_{si})\}$, but it cannot distinguish the aliasing frequencies of a certain true frequency f_k from $\mathbb{S}_1, \cdots, \mathbb{S}_S$.

3. Delay coprime sampling scheme

Here, we consider a special PNS with two low-rate channels:

$$\begin{aligned} y_1[n] &\triangleq x[nL] = x(nLT), \\ y_2[n] &\triangleq x[nL+P] = x(nLT+PT), \end{aligned} \tag{6}$$

where T denotes the nominal (unit) interval, typically Nyquist interval. LT denotes the sampling period of each channel. PT is delay between two channels, which can be precisely controlled by clock signal triggering [31]. Particularly, L and P are coprime integers, i.e., $\gcd\{L,P\}=1$, as shown in Fig. 3. This sampling is throughout referred to as DCS [32]. Furthermore, let $Q \triangleq (L-P)$, then we have $\gcd\{P,Q\} = \gcd\{L,Q\} = 1$ which can be easily proven by contradiction.

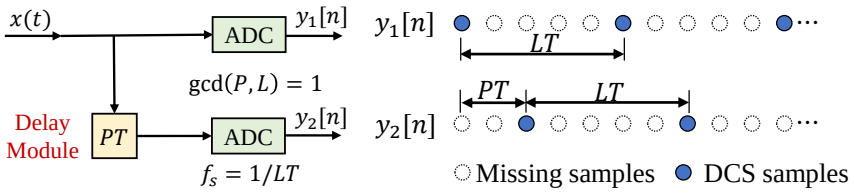

(a) (b)

Figure 3: DCS: (a) system prototype and (b) sampling process.

The average sampling rate of DCS is given in

$$\bar{f}_s^{DCS} = \frac{2}{P+Q} f_{\text{Nyq}}, \tag{7}$$

where f_{Nyq} denotes the Nyquist rate, $f_{\text{Nyq}} \triangleq 1/T$.

3.1. Equivalent sampling and aliasing frequencies pair

Because DCS does not physically implement multi-rate sampling, we set out to collect aliasing frequency by the phase change caused by delay. Note that, although the following derivation is performed in the continuous domain, the extension to the discrete domain is straightforward.

Given two identical signals with delay τ: $y_1(t) = x(t), y_2(t) = x(t+\tau)$, we obtain

$$\tilde{\boldsymbol{Y}}_2(f) = \tilde{\boldsymbol{Y}}_1(f) e^{j2\pi f\tau}, \tag{8}$$

where $\tilde{\boldsymbol{Y}}_1(f)$ and $\tilde{\boldsymbol{Y}}_2(f)$ denote the true spectra of $y_1(t)$ and $y_2(t)$, respectively. Assuming that f_t is a true frequency in the spectrum, we apparently have $\tilde{\boldsymbol{Y}}_2(f_t) = \tilde{\boldsymbol{Y}}_1(f_t) e^{j2\pi f_t\tau}$. Next, the phase difference ϕ between $\tilde{\boldsymbol{Y}}_1(f_t)$ and $\tilde{\boldsymbol{Y}}_2(f_t)$ can be calculated by

$$\phi \triangleq \underset{[0,2\pi)}{\text{angle}} \left(\tilde{\boldsymbol{Y}}_1^*(f_t) \tilde{\boldsymbol{Y}}_2(f_t) \right) \overset{(o)}{=} \underset{[0,2\pi)}{\text{angle}} \left(\boldsymbol{Y}_1^*(f_a) \boldsymbol{Y}_2(f_a) \right), \tag{9}$$

where $\underset{[0,2\pi)}{\text{angle}}(\cdot)$ is a phase angle operator defined in (10) which maps each complex number to a phase angle within $[0, 2\pi)$. (o) comes from the fact that $\tilde{\boldsymbol{Y}}_i(f_t) = \boldsymbol{Y}_i(f_a)$ for $i = 1, 2$, as shown in Fig. 1. In the case of sub-Nyquist sampling, although $\tilde{\boldsymbol{Y}}_i(f_t)$ is unavailable, $\boldsymbol{Y}_i(f_a)$ can be computed from discrete samples; thus,

(8) and (9) imply that the true frequency can be estimated by $\phi/(2\pi\tau)$, which is the prototype of time delay estimation (TDE) [33]. Because $\phi \in [0, 2\pi)$, it is necessary for frequency estimation that the delay τ should be smaller than the Nyquist interval, i.e., $\tau < 1/f_{\max}$. Restricted by this condition, delay τ in TDE is usually very small. An extremely small τ will significantly amplify the error of phase (difference) estimation and results in huge frequency estimation error [34, 35]. Therefore, TDE is impractical due to its small delay. To improve the robustness to measurement noise and phase errors, active aliasing technique [36], i.e., AATDE, is employed in this manuscript. Specifically, different from TDE, AATDE uses a delay larger than the Nyquist interval to calculate frequency.

$$\underset{[0,2\pi)}{\text{angle}}(a+bj) = \begin{cases} \tan^{-1}\left(\frac{b}{a}\right) & a>0, b\geqslant 0 \\ \tan^{-1}\left(\frac{b}{a}\right)+2\pi & a>0, b<0 \\ \tan^{-1}\left(\frac{b}{a}\right)+\pi & a<0 \\ \frac{b}{|b|}\frac{\pi}{2} & a=0, b>0 \\ \frac{b}{|b|}\frac{3\pi}{2} & a=0, b<0 \\ 0 & a=0, b=0 \end{cases}, \tag{10}$$

where $(a+bj)$ denotes a complex number.

Let τ_i be a delay larger than the Nyquist interval, we have

$$\tilde{f}_{ai} = \frac{\phi}{2\pi\tau_i} = \frac{\phi}{2\pi}\tilde{f}_{si},\ i=1,2,3, \tag{11}$$

where $\tau_i < 1/f_t$; thus, $\frac{\phi}{2\pi\tau_i}$ is the aliasing result of the true frequency f_t, denoted by equivalent aliasing frequency $\tilde{f}_{ai}$. $\tilde{f}_{si}$ denote the equivalent sampling frequency, $\tilde{f}_{si} \triangleq 1/\tau_i$. Numerically, $\tilde{f}_{ai}$ is equal to the aliasing frequency of f_t when $f_s = \tilde{f}_{si}$, i.e., $\tilde{f}_{ai} = \text{mod}(f_t, \tilde{f}_{si})$. This finding prompts us to diversify delay τ_i to enrich aliasing information and then reconstruct f_t. By using different delays τ_i, we equivalently implement multi-rate sampling instead of physically, which significantly simplifies the hardware configuration. To emphasize this equivalent implementation, $\tilde{f}_{ai}$ and $\tilde{f}_{si}$ are called equivalent aliasing frequency and equivalent sampling frequency, respectively. Note that, $\tilde{f}_{ai}$ obtained by (11) is not limited to the fixed frequency grids, this gridless nature is helpful to improve accuracy estimation.

3.2. Delay scheme constructed by changing selected data

In DCS, we can flexibly construct delay schemes by changing selected data sequences, as shown in Fig. 4, where the two data sequences in the dashed boxes denotes the input data for aliasing frequency estimation. Firstly, we construct the first delay scheme by selecting the two data sequences as follows

$$\text{Scheme 1:}\ \begin{cases} \boldsymbol{y}_1' = [y_1[0], y_1[1], \cdots, y_1[N-1]]^{\mathrm{T}} \\ \boldsymbol{y}_2' = [y_2[0], y_2[1], \cdots, y_2[N-1]]^{\mathrm{T}} \end{cases},$$

where $\boldsymbol{y}_1'$ and $\boldsymbol{y}_2'$ denote the selected data sequences for equivalent aliasing frequency estimation. The sampling time difference between $\boldsymbol{y}_1'$ and $\boldsymbol{y}_2'$ is referred as to delay. Readily, the delay and equivalent sampling frequency in the first scheme are

$$\tau_1 = PT,\ \tilde{f}_{s1} = \frac{1}{\tau_1} = \frac{1}{PT} = \frac{f_{\text{Nyq}}}{P}.$$

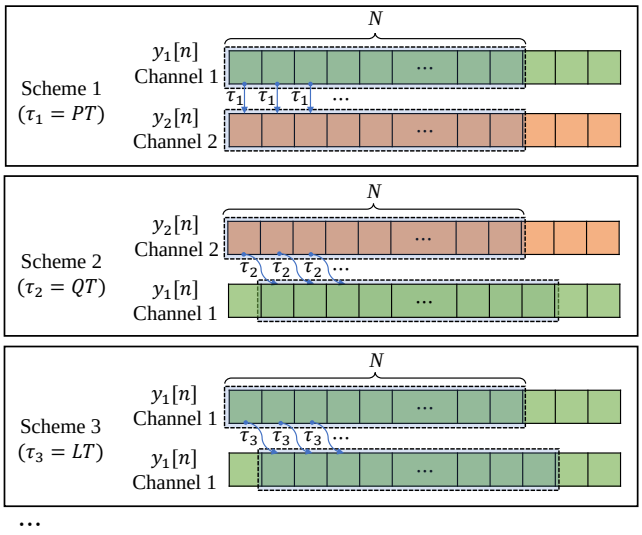

Figure 4: Schematic diagram of different delay schemes. Note that we only list the first three delay schemes for brevity.

Then, the second delay scheme is constructed as follows

$$\text{Scheme 2:} \begin{cases} \boldsymbol{y}_1' = [y_2[0], y_2[1], \cdots, y_2[N-1]]^{\mathrm{T}} \\ \boldsymbol{y}_2' = [y_1[1], y_1[2], \cdots, y_1[N]]^{\mathrm{T}} \end{cases}$$

In the second scheme,

$$\tau_2 = QT, \ \tilde{f}_{s2} = \frac{1}{\tau_2} = \frac{1}{QT} = \frac{f_{\mathrm{Nyq}}}{Q}.$$

Similarly, the third delay scheme is constructed as follows

$$\text{Scheme 3:} \begin{cases} \boldsymbol{y}_1' = [y_1[0], y_1[1], \cdots, y_1[N-1]]^{\mathrm{T}} \\ \boldsymbol{y}_2' = [y_1[1], y_1[2], \cdots, y_1[N]]^{\mathrm{T}} \end{cases}.$$

In the third scheme,

$$\tau_3 = LT, \ \ \tilde{f}_{s3} = \frac{1}{\tau_3} = \frac{1}{LT} = \frac{f_{\mathrm{Nyq}}}{L}.$$

It is readily seen that the other delays equal the first three delays plus an integer multiple of LT. *In this paper, we mainly focus on the first three delays schemes* and the extension to other larger delay case is straightforward. After determining the data sequences with τ_i for $i = 1, 2, 3$, we can calculate the equivalent aliasing frequency $\tilde{f}_{ai}$ using the method given in Section 3.1. As a summary, the algorithm flow for mining aliasing information is as follows

3.3. Comparison to coprime sampling

In this subsection, we explain the advantage of DCS by comparing it with a prevalent sub-Nyquist sampling scheme (CS)[4]. CS exploits two uniform sub-Nyquist samplers with sampling period being coprime multiples of

[4]We only compare the DCS and CS themselves as well as the corresponding methods for mining aliasing information. The ability of CS for power spectrum estimation is not considered here.

Algorithm 1: AATDE

Input: $\boldsymbol{y}_1, \boldsymbol{y}_2$: data from DCS; N: data length for DFT; K: the number of frequencies.

Output: sampling and aliasing frequency pairs;

1 Generate delay schemes, $\tau_1, \cdots, \tau_S$ and equivalent sampling frequencies, $\tilde{f}_{s1}, \cdots, \tilde{f}_{sS}$;

2 Select the data $\boldsymbol{y}_1'$ and $\boldsymbol{y}_2'$ according to the delay scheme, τ_i, $1 \leqslant i \leqslant S$;

3 Calculate Fourier coefficients of $\boldsymbol{y}_1'$ and $\boldsymbol{y}_2'$, denoted by $\boldsymbol{Y}_1$ and $\boldsymbol{Y}_2$;

4 Find the location index set $\mathbb{L}$ of the most significant K peaks in amplitude spectrum $|\boldsymbol{Y}_1|$;

5 Calculate the equivalent aliasing frequencies of the lth index, $\tilde{f}_{ai}(l) = \underset{[0,2\pi)}{\text{angle}}\left(\boldsymbol{Y}_1^*(l)\boldsymbol{Y}_2(l)\right) / \left(2\pi\tau_i\right)$, $\forall l \in \mathbb{L}$.

T. The sampling model of CS is

$$\begin{aligned} y_1[k] &\triangleq x[Uk] = x(UkT), \\ y_2[k] &\triangleq x[Vk] = x(VkT), \end{aligned} \tag{12}$$

where $\gcd\{U, V\} = 1$. Obviously, this CS is equivalent to a PNS of order $(U + V)$ where the sampling rate of each channel is $f_{\text{Nyq}}/(UV)$. It follows that the average sampling rate of CS is

$$\bar{f}_s^{CS} = \frac{U+V}{UV} f_{\text{Nyq}}. \tag{13}$$

Table 1 lists the key comparison of DCS and CS. Based on this table, we briefly explain the advantages of DCS over CS in applicability by considering their abilities in overcoming the following two challenges. **Challenge 1: From complex-valued waveforms to real-valued waveforms.** When the signal is a real-valued waveform, there exists ambiguity between (equivalent) aliasing frequencies and remainders, leading to nonunique solutions. For CS, additional hardware, e.g., a triggering circuit for zero-crossing detection [28] or an added sub-Nyquist sampler for grouping operations, is required to eliminate this ambiguity. However, DCS can be directly applied to real-valued waveforms using grouping operations, the details can be found in Section 5. **Challenge 2: From a single frequency to multi-frequency.** When the signal has multiple frequencies, there exists ambiguity between multiple frequencies and their aliasing frequencies, which leads to unacceptable complexity. Existing CRT-based reconstruction is generally only applicable to single-frequency or two-frequencies cases and ineffective for multiple-frequencies cases unless the amplitude difference between different frequencies is significant enough to distinguish themselves. However, the multiple frequencies and their equivalent aliasing frequencies do clearly correspond in AATDE as long as the aliasing results of multiple frequencies are separate. Therefore, in the proposed method, the multi-frequency estimation problem can be naturally simplified to multiple independent single-frequency estimations, which can be efficiently achieved. Relevant textual and graphic explanations can be found in Section 6. Furthermore, according to the principle of AATDE, the key prerequisite to obtaining aliasing frequencies of multiple true frequencies without ambiguity is an amplitude spectrum with significant aliasing peaks. That is, the aliasing peaks in the amplitude spectrum are required to be separated and significant. Therefore, our method is based on the sparse signal assumption, and it requires that the aliasing peaks of true frequencies in the amplitude spectrum at sub-Nyquist rate $f_s = f_{\text{Nyq}}/L$ are distinguishable.

Table 1: Comparison of DCS and CS.

Description	DCS (P, Q)	CS (U, V)
Average sampling rate	$\frac{2}{P+Q} f_{\text{Nyq}}$	$\frac{U+V}{UV} f_{\text{Nyq}}$
Remainders are generated by	AATDE	DFT
Number of congruence equations	$\geqslant 2$	$= 2$
Real-valued waveform case	Applicable	Hardware dependent
Multiple frequencies case	Easy	Complicated

4. Frequency estimation for complex-valued waveforms

In this section, we use the CRT-based algorithm [18, 23] to reconstruct the true frequency from aliasing findings. Corresponding conclusions are actually the straightforward corollaries of the theorems in [18, 23].

4.1. Congruence equations and reconstruction algorithm

Numerically, $\tilde{f}_{ai}$ equals the aliasing result of f_t in the case of $f_s = \tilde{f}_{si}$. (P.S. There will always be errors in practice which will be discussed in the next subsection.) Remarkably, we implement equivalent multi-rate sampling by changing delay/phase. Therefore, $\tilde{f}_{si}$ and $\tilde{f}_{ai}$ are termed equivalent sampling frequency and aliasing frequency, respectively. $\tilde{f}_{ai}$ equals the aliasing result of f_t in the case of $f_s = \tilde{f}_{si}$; thus, following the aliasing law of complex-valued signal, we obtain

$$\text{mod}(f_t, \tilde{f}_{si}) = \tilde{f}_{ai} \text{ or } f_t = n_i \tilde{f}_{si} + \tilde{f}_{ai} \text{ for } i = 1, 2, 3. \tag{14}$$

Before proceeding, for ease of the description, we give some generalized definitions as follows

Definition 1 (generalized coprime number and generalized greatest common divisor). *If a and b are coprime integers, then ma and mb are called generalized coprime number where $m \in \mathbb{R}$ is referred to as generalized greatest common divisor. Particularly, m is denoted by* $\text{ggcd}\{ma, mb\}$.

Definition 2 (generalized least common multiple). *If some real numbers $a_1, a_2, \cdots, a_S$ that can be integers by dividing a constant b, i.e., $a_i/b \in \mathbb{N}$, $b \cdot \text{lcm}\{a_1/b, \cdots, a_S/b\}$ is defined as their generalized least common multiple, denoted by* $\text{glcm}\{a_1, a_2, \cdots, a_S\}$.

Here are some demonstrative examples for definitions 1 and 2 for clarity. For example, 0.2 and 0.3 can be coprime integers $(2, 3)$ by dividing 0.1. Thus, they are generalized coprime numbers and $\text{ggcd}\{0.2, 0.3\} = 0.1$. For example, 0.1, 0.2, and 0.3 can be integers by dividing 0.1; thus, $\text{glcm}\{0.1, 0.2, 0.3\} = 0.1 \cdot \text{lcm}\{1, 2, 3\} = 0.6$.

Then, we set out to reconstruct the true frequency f_t from (14). Note that (14) is a congruence equation which can be analyzed by CRT. According to CRT, we have a corollary:

Corollary 1. *Let $\tilde{f}_{si}$, $1 \leqslant i \leqslant S$, be S arbitrarily positive numbers as moduli. The target frequency can be uniquely reconstructed from (14) if* $0 \leqslant f < \text{glcm}\{\tilde{f}_{s1}, \tilde{f}_{s2}, \cdots, \tilde{f}_{sS}\}$.

Corollary 1 is a straightforward corollary of CRT, which extends the moduli and the reconstructed target from the integer domain to the real domain to improve its practicality.

Then, we analyze the maximum frequency that can be reconstructed in theory, i.e., $\text{glcm}\{\tilde{f}_{s1}, \tilde{f}_{s2}, \cdots, \tilde{f}_{sS}\}$. The analysis result is formally presented as follows

Theorem 1. *The supremum frequency f_{sup} that can be uniquely identified/reconstructed by solving the congruence equations (14) is $1/T$, i.e., f_{Nyq}, in the complex-valued case.*

Next, we consider a specific CRT-based reconstruction algorithm to solve (14). In this paper, we use the robust algorithm proposed in [18, 23] to reconstruct f_t by solving (14). The specific algorithm flow is illustrated in Algorithm 2.

Algorithm 2: CR-CRT [18, 23]

Input: $\{\tilde{f}_{si}\}_{i=1}^{S}$: moduli; $\{\tilde{f}_{ai}\}_{i=1}^{S}$: erroneous remainders.

Output: $\hat{f}_t$:the frequency to be reconstructed.

1 Calculate $\hat{q}_{i1}$ for $2 \leqslant i \leqslant S$: $\hat{q}_{i1} \leftarrow \left[\frac{(\tilde{f}_{ai}-\tilde{f}_{a1})}{m_{1i}}\right]$ where $m_{1i} = \text{ggcd}\{\tilde{f}_{s1}, \tilde{f}_{si}\}$ and $[\cdot]$ denotes the rounding integer;

2 Calculate the remainders of $\hat{q}_{i1}\bar{\Gamma}_i$ modulo Γ_{i1}, $\hat{\xi}_{i1} \leftarrow \text{mod}(\hat{q}_{i1}\bar{\Gamma}_i, \Gamma_{i1})$ where $\bar{\Gamma}_i$ is the modular multiplicative inverse of Γ_{1i} modulo Γ_{i1};

3 Calculate $\hat{n}_1$ by solving the congruence equations, $\hat{\xi}_{i1} = \text{mod}(\hat{n}_1, \Gamma_{i1})$, $2 \leqslant i \leqslant S$;

4 Calculate $\hat{n}_i$ for $2 \leqslant i \leqslant S$: $\hat{n}_i = (\hat{n}_1\Gamma_{1i} - \hat{q}_{i1})/\Gamma_{i1}$;

5 Reconstruct the target, $\hat{f}_t = \frac{1}{S}\sum_{i=1}^{S} \hat{n}_i\tilde{f}_{si} + \tilde{f}_{ai}$.

4.2. Error tolerance bound

In practice, remainder errors are inevitable. In this subsection, we consider the influence of remainder error (equivalent aliasing frequency error) on the reconstruction algorithm.

According to [23], we obtain the following theorem

Theorem 2: *The folding number n_i can be accurately determined if and only if*

$$\left|\Delta\tilde{f}_{ai} - \Delta\tilde{f}_{a1}\right| \leqslant \text{ggcd}\{\tilde{f}_{s1}, \tilde{f}_{si}\}/2, \tag{15}$$

where $\Delta\tilde{f}_{ai}$ denotes the error of $\tilde{f}_{ai}$, $\tilde{f}^*_{ai} = \tilde{f}_{ai} + \Delta\tilde{f}_{ai}$, $\tilde{f}^*_{ai}$ is the ith accurate aliasing frequency.

Although condition (15) is necessary and sufficient for the uniqueness of the solution of the folding integers from CR-CRT, it involves two remainder errors and is hard to check in practice. Below, we present a simpler sufficient condition.

Corollary 2. *If each remainder error, i.e., $\Delta\tilde{f}_{ai}$ satisfies*

$$\left|\Delta\tilde{f}_{ai}\right| < \max_{1\leqslant k\leqslant S} \min_{1\leqslant j\neq k\leqslant S} \frac{\text{ggcd}\{\tilde{f}_{sk}, \tilde{f}_{sj}\}}{4}, \tag{16}$$

then the folding integers n_i can be accurately determined.

The proof of Corollary 2 is presented in Appendix C.

5. Extension to real-valued waveforms

Different from the complex waveform, a sinusoidal real-valued waveform is the superposition of two conjugate complex waveforms,

$$\cos(2\pi f_k t + \varphi_k) = \frac{1}{2}\left(e^{j(2\pi f_k t+\varphi_k)} + e^{-j(2\pi f_k t+\varphi_k)}\right), \tag{17}$$

which indicates a real-valued signal contains symmetric peaks in the spectrum. Thus, the real-valued waveform has an additional negative duplicate compared to the complex-valued case. In this case, the proposed DCS is still effective by incorporating grouping operations. However, due to the presence of the negative duplicate, the supremum frequency that can be identified is half of the original, i.e., $f_{\text{sup}} = f_{\text{Nyq}}/2$, in the real-valued case. The following is the specific introduction.

For a real-valued sinusoidal signal with frequency f_t, there exist two aliasing results in the range $[0, f_s)$ in the case of sub-Nyquist sampling ($f_s < 2f_t$), which are caused by the periodic extension of f_t and $-f_t$, respectively. However, the correspondence is ambiguous. In the real-valued signal case, the aliasing result in the first Nyquist zone $[0, f_s/2)$ is traditionally referred to as aliasing frequency of f_t, which can be equivalently calculated by

$$\tilde{f}_{ai} = \frac{|\phi|}{2\pi\tau_i} = \frac{|\phi|}{2\pi}\tilde{f}_{si},\ i = 1, 2, 3, \tag{18}$$

where ϕ is the phase difference defined as

$$\phi = \underset{(-\pi,\pi]}{\text{angle}}\left(\boldsymbol{Y}_1^*(f_a)\boldsymbol{Y}_2(f_a)\right), \tag{19}$$

where $\underset{(-\pi,\pi]}{\text{angle}}(\cdot)$ is a phase angle operator defined in (20) which maps each complex number to a phase angle within $(-\pi, \pi]$. Note that, the calculation of $\tilde{f}_{ai}$ in real-valued signals [(18)$\sim$(20)] is different from that in complex-valued signals [(9)$\sim$(11)].

$$\underset{(-\pi,\pi]}{\text{angle}}(a+bj) = \begin{cases} \tan^{-1}\left(\frac{b}{a}\right) & a > 0 \\ \tan^{-1}\left(\frac{b}{a}\right) + \pi & a < 0, b \geqslant 0 \\ \tan^{-1}\left(\frac{b}{a}\right) - \pi & a < 0, b < 0 \\ \frac{b}{|b|}\frac{\pi}{2} & a = 0, b \neq 0 \\ 0 & a = 0, b = 0 \end{cases}. \tag{20}$$

5.1. Congruences grouping

The frequency f_t in real-valued signal follows the following aliasing law in the case of sub-Nyquist sampling,

$$f_a = \min_{m\in\mathbb{N}} |f_t - mf_s| = \min\left\{\text{mod}(f_t, f_s), f_s - \text{mod}(f_t, f_s)\right\}, \tag{21}$$

where m is the integer that minimizes $|f_t - mf_s|$, and the corresponding minimum is defined as f_a, $f_a \in [0, f_s/2)$. Numerically, f_a equals the minimum of $\text{mod}(f_t, f_s)$ and $f_s - \text{mod}(f_t, f_s)$.

With the same reasoning, the $\tilde{f}_{ai}$ obtained by AATDE is equivalent to the aliasing result of f_t in the case of $f_s = \tilde{f}_{si}$; thus, we have

$$\tilde{f}_{ai} = \min_{\kappa\in\mathbb{N}} |f_t - \kappa\tilde{f}_{si}| = \min\{\text{mod}(f_t, \tilde{f}_{si}), \tilde{f}_{si} - \text{mod}(f_t, \tilde{f}_{si})\}, \tag{22}$$

where κ is the integer that minimizes $|f_t - \kappa\tilde{f}_{si}|$.

In the congruence equation of CRT, the ith remainder is defined as $\text{mod}\,(f_t, \tilde{f}_{si})$ where f_t is the frequency to be reconstructed and $\tilde{f}_{si}$ is the modulus. In the complex-valued case, the aliasing law follows $\tilde{f}_{ai} = \text{mod}\,(f_t, \tilde{f}_{si})$;

thus, $\tilde{f}_{ai}$ is equal to the remainder. However, in any real-valued case, the remainder denoted by $\tilde{r}_{ai} \triangleq \text{mod}(f_t, \tilde{f}_{si})$ has two possible values from (22), i.e.,

$$\tilde{r}_{ai} = \begin{cases} \tilde{f}_{ai} & f_t = \kappa \tilde{f}_{si} + \tilde{f}_{ai} \\ \tilde{f}_{si} - \tilde{f}_{ai} & f_t = \kappa \tilde{f}_{si} - \tilde{f}_{ai} \end{cases}. \tag{23}$$

Due to the ambiguity of remainder, f_t cannot be directly reconstructed by CR-CRT. To eliminate the ambiguity, a grouping strategy is utilized. First, the S congruence equations are divided into $\mathrm{C}_S^2 = \frac{S!}{2!(S-2)!}$ groups. For example, we present the groups in the case of $S = 3$ in (24).

$$\begin{cases} \text{mod}(f_t, \tilde{f}_{s1}) = \tilde{r}_{a1} \\ \text{mod}(f_t, \tilde{f}_{s2}) = \tilde{r}_{a2} \end{cases}, \begin{cases} \text{mod}(f_t, \tilde{f}_{s1}) = \tilde{r}_{a1} \\ \text{mod}(f_t, \tilde{f}_{s3}) = \tilde{r}_{a3} \end{cases}, \begin{cases} \text{mod}(f_t, \tilde{f}_{s2}) = \tilde{r}_{a2} \\ \text{mod}(f_t, \tilde{f}_{s3}) = \tilde{r}_{a3} \end{cases}. \tag{24}$$

Estimates of f_t can be calculated from the congruence equations in each group. When remainders are accurately selected, the estimates are valid if the remainder errors are below the tolerance. However, when remainders are mistakenly selected, remainder errors must have exceeded the tolerance and the estimates are invalid. For S known equivalent aliasing frequencies, $\tilde{f}_{a1}, \tilde{f}_{a2}, \cdots, \tilde{f}_{aS}$, there exist 2^S possible combinations of remainders $\{\tilde{r}_{a1}, \tilde{r}_{a2}, \cdots, \tilde{r}_{aS}\}$. Then, we consider all combinations and estimate f_t by solving the congruence equation groups. Note that, time-complexity of the proposed method increases exponentially with S. Furthermore, the delays after the first three has smaller remainder error tolerances, thus have higher failure risk in frequency reconstruction. Considering the negligible accuracy improvement, high failure risk, and huge computational complexity caused by increasing S, it is recommended to use the first three delays, i.e., $S = 3$.

5.2. Frequency estimations sifting

Next, we begin to sift the frequency estimations and select the valid estimations. When the remainders are correctly selected, the estimates from the congruence equations are valid estimates of the true frequency. When the remainders are mistakenly selected, the estimates are invalid estimates of the true frequency and there exists at least one outlier. Therefore, the estimations from the correct remainder combinations exhibit high consistency. Specifically, we used the following criterion to sift frequency estimations.

Consistency criterion: The frequency estimations with minimum variance are considered the valid estimation of target frequency, as follows

$$\hat{f}_t = \arg\min_{\hat{f}_{tc}} \sum\nolimits_{i=1}^{3} \left(\hat{f}_{tc}(i) - \bar{f}_{tc} \right)^2, \tag{25}$$

where $\hat{f}_{tc}(i)$ denotes the frequency estimation from the ith congruence equation group in the case of the cth remainder combination. $\bar{f}_{tc}$ is the average of the frequency estimations, $\bar{f}_{tc} = \frac{1}{3} \sum_{i=1}^{3} \hat{f}_{tc}(i)$.

However, it should be claimed that **consistency criterion** cannot uniquely determine the valid frequency estimations. There always exist two remainder combinations that result in two frequency estimation sets with the same minimum variance. The detailed explanation on this assertion can be found in the proof of Theorem 3 (Appendix D). In order to uniquely determine the valid frequency estimation, we rely on an additional criterion:

Minimum estimation criterion: Calculate the respective averages of the two set estimations with the smallest variance obtained by the consistency criterion and choose the minimum average as the final frequency estimation, i.e.,

$$\hat{f}_t = \min\{\bar{f}_{tc_1}, \bar{f}_{tc_2}\}, \tag{26}$$

where $\bar{f}_{tc_1}$ and $\bar{f}_{tc_2}$ denote the averages of the two set estimations sifted by the consistency criterion, respectively.

Note that the above **minimum estimation criterion** depends on the prerequisite that $f_t \leqslant f_{\text{Nyq}}/2$. That is, the target frequency to be estimated by the proposed method cannot exceed $f_{\text{Nyq}}/2$, otherwise, the method will fail. This assertion comes from the following theorem.

Theorem 3. *The supremum frequency f_{sup} that can be uniquely identified by solving the congruence equation groups (24) is $1/(2T)$, i.e., $f_{\text{Nyq}}/2$, in the real-valued case.*

The proof of Theorem 3 is presented in Appendix D.

In a nutshell, in order to apply to the real-valued signal case, grouping operation and frequency sifting operation are added to CR-CRT, as summarized in Algorithm 3.

Algorithm 3: Grouping and Sifting CR-CRT (GSCR-CRT)

Input: $\{\tilde{f}_{si}\}_{i=1}^{3}$: moduli; $\{\tilde{f}_{ai}\}_{i=1}^{3}$: erroneous remainders.

Output: $\hat{f}_t$:the frequency to be reconstructed.

1 Group congruence equations according to (24);

2 Solve congruence equations from each group and obtain frequency estimations $\hat{f}_{tc}(g)$ by CR-CRT where $c = 1, 2, \cdots, 8$ and $g = 1, 2, 3.$;

3 Sift frequency estimations by consistency criterion and minimum estimation criterion.

For the ease of understanding, we provide an example.

Example: Assume that the target frequency f_t of the real-valued signal is 100 MHz, and $T = 1/210$ μs, $f_{\text{Nyq}} = 210$ MHz. DCS ($P = 3, Q = 7$) is employed to acquire the samples (Note that the average sampling rate of the DCS is only 42 MHz). In this case, the first three available delay schemes are $\{3T, 7T, 10T\}$. Accordingly, $\{\tilde{f}_{s1}, \tilde{f}_{s2}, \tilde{f}_{s3}\} = \{70, 30, 21\}$. This example is to show how GSCR-CRT reconstructs the true frequency from $\{\tilde{f}_{si}, \tilde{f}_{ai}\}_{i=1}^{3}$. For demonstration purpose, the equivalent aliasing frequencies are assumed to be error-free here. Theoretically, we can obtain $\{\tilde{f}_{a1}, \tilde{f}_{a2}, \tilde{f}_{a3}\} = \{30, 10, 5\}$. According to (23), we have the following 8 possible combinations of $\{\tilde{r}_{a1}, \tilde{r}_{a2}, \tilde{r}_{a3}\}$, as shown in Table 2. By the **consistency criterion**, we can locate the combinations 2 and 7. Their estimated results are 100 and 110 MHz, respectively. On this basis, by the **minimum estimation criterion**, 100 MHz is considered the final estimate of f_t. Obviously, f_t can be successfully estimated by the proposed method in the real-valued case.

As a summary, the complete flow-graph of the proposed method is given in Fig. 5. The proposed method is based on DCS, and it can deal with complex-valued and real-valued multi-frequency signals using CR-CRT and GSCR-CRT algorithms, respectively. Table 3 lists the comparison between the proposed method and CS-based method.

Table 2: An example for demonstrating frequency estimation sifting.

No.	$\tilde{r}_{a1}$	$\tilde{r}_{a2}$	$\tilde{r}_{a3}$	$\hat{f}_t(1)$	$\hat{f}_t(2)$	$\hat{f}_t(3)$
1	30	10	5	100	171.5	130.5
2	30	10	16	100	100	100
3	30	20	5	170	171.5	110
4	30	20	16	170	100	79.5
5	40	10	5	40	110	130.5
6	40	10	16	40	38.5	100
7	40	20	5	110	110	110
8	40	20	16	110	38.5	79.5

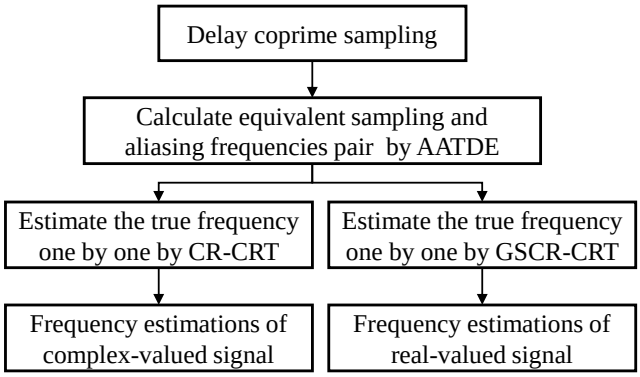

Figure 5: The flow-graph of the proposed method.

Table 3: Comparison of the different methods.

Method	CR-CRT with DCS	GSCR-CRT with DCS	CR-CRT with CS
Complexity	$O(2SN\log N + KN)$ $+\mathrm{C}_S^2 \cdot O(2\log^2 L)$ $\overset{S=3}{\approx} O(6N\log N + KN)$	$O(SN\log N + KN)$ $+2^S \cdot \mathrm{C}_S^2 \cdot O(2\log^2 L)$ $\overset{S=3}{\approx} O(3N\log N + KN)$	$O(UN\log(UN) + KUN)$ $+O(VN\log(VN) + KVN)$ $+O(2\log^2 L)$
Applicability	Complex-valued signal Multi-frequency	Real-valued signal Multi-frequency	Complex-valued signal Single-frequency

Corollary 3. *In the real-valued waveform case, if the target frequency* $f_t \in [0, f_{\mathrm{Nyq}}/2]$ *and each remainder error, i.e.,* $\Delta\tilde{f}_{ai}$*, satisfies*

$$|\Delta\tilde{f}_{ai}| < \frac{1}{4}\min\left\{\frac{f_{\mathrm{Nyq}}}{PQ}, \frac{f_{\mathrm{Nyq}}}{PL}, \frac{f_{\mathrm{Nyq}}}{QL}\right\},\ i = 1, 2, 3, \tag{27}$$

then the folding integers n_i *can be accurately determined and the error bound of target frequency estimation is* $\frac{\sqrt{3}}{12}\min\left\{\frac{f_{\mathrm{Nyq}}}{PQ}, \frac{f_{\mathrm{Nyq}}}{PL}, \frac{f_{\mathrm{Nyq}}}{QL}\right\}$.

According to Theorem 1 and Theorem 3, we derive a necessary condition for identifiability in DCS scheme:

$$\begin{cases} L \cdot f_s > f_{\max} & \text{complex} \\ L \cdot f_s \geqslant 2f_{\max} & \text{real} \end{cases}, \tag{28}$$

where $f_{\max}$ denotes the maximum frequency of the signal. f_s is the sampling rate of each channel in DCS.

By Corollary 3, we can improve the probability of successful reconstruction by optimizing DCS, i.e., the configuration of P, Q, and L. According to Corollary 3, we should increase the error tolerance bound, i.e., $\frac{1}{4}\min\left\{\frac{f_{\text{Nyq}}}{PQ}, \frac{f_{\text{Nyq}}}{PL}, \frac{f_{\text{Nyq}}}{QL}\right\}$, as much as possible. Assuming L is given and it satisfies the identifiability condition (28), we have the optimization model for DCS,

$$\min \max\{P,Q\}, \text{ s.t.} \begin{cases} P+Q=L \\ \gcd\{P,Q\}=1 \\ 1 \leqslant P,Q \leqslant L-1 \end{cases}. \tag{29}$$

For a given L larger than 2, the optimal configuration is

$$\begin{cases} P=\frac{L-1}{2}, Q=\frac{L+1}{2} & L \text{ is odd} \\ P=\frac{L-2}{2}, Q=\frac{L+2}{2} & \gcd\{L,4\}=4 \\ P=\frac{L-4}{2}, Q=\frac{L+2}{2} & \gcd\{L,4\}=2 \end{cases}, \tag{30}$$

where the case of even L is divided into two sub-cases: $\gcd\{L,4\}=4$ and $\gcd\{L,4\}=2$.

5.3. Performance analysis

5.3.1. Comparison to CR-CRT

CR-CRT does not involve grouping and sifting operations; thus, it cannot eliminate the ambiguity of remainder due to negative duplicate and is ineffective for real-valued signal analysis. In contrast, owing to the grouping operations, the first advantage of the proposed algorithm is that it can eliminate the ambiguity of remainder and determine the valid estimation of target frequency based on the consistency criterion and minimum estimation criterion. Furthermore, coprime property of delays in DCS, the supremum frequency f_{sup} does not decrease due to grouping operations. Specifically, the frequency range that can be uniquely determined by solving the complete congruence equations $\text{mod}(f_t, \tilde{f}_{si}) = \tilde{f}_{ai}$ for $1 \leqslant i \leqslant 3$ is $0 \leqslant f_t < \text{glcm}\{\tilde{f}_{s1}, \tilde{f}_{s2}, \tilde{f}_{s3}\} = f_{\text{Nyq}}$; The frequency range that can be uniquely determined by solving each grouped congruence equation (24) is $0 \leqslant f_t < \text{glcm}\{\tilde{f}_{s1}, \tilde{f}_{s2}\} = \text{glcm}\{\tilde{f}_{s1}, \tilde{f}_{s3}\} = \text{glcm}\{\tilde{f}_{s2}, \tilde{f}_{s3}\} = f_{\text{Nyq}}$, which is the same as the previous result. It should be claimed that the halving of f_{sup} in the real-valued signal is not caused by the grouping operations but by the ambiguity of the remainder (the presence of negative frequency). Then, we compare the error tolerance bound of the remainder before and after grouping. Without loss of generality, let $P \leqslant Q$. According to Corollary 2, the remainder error bound of complete congruence equations $\text{mod}(f_t, \tilde{f}_{si}) = \tilde{f}_{ai}$ for $1 \leqslant i \leqslant 3$ is $\frac{1}{4}\frac{f_{\text{Nyq}}}{PL}$, whereas the remainder error bound of grouped congruence equations (24) is $\frac{1}{4}\min\left\{\frac{f_{\text{Nyq}}}{PQ}, \frac{f_{\text{Nyq}}}{PL}, \frac{f_{\text{Nyq}}}{QL}\right\} = \frac{1}{4}\frac{f_{\text{Nyq}}}{QL}$ by Corollary 3. Obviously, the remainder error tolerance bound is reduced due to the grouping operations in this paper. In the optimal configuration of DCS given in (30), the reduction is

$$\frac{1}{4}\frac{f_{\text{Nyq}}}{PL} - \frac{1}{4}\frac{f_{\text{Nyq}}}{QL} = \begin{cases} \frac{f_{\text{Nyq}}}{L^3-L} & L \text{ is odd} \\ \frac{2f_{\text{Nyq}}}{L^3-4L} & \gcd\{L,4\}=4 \\ \frac{4f_{\text{Nyq}}}{L^3-16L} & \gcd\{L,4\}=2 \end{cases}. \tag{31}$$

Eq. (31) indicates the reduction of the remainder error tolerance bound due to grouping operation is negligible as L increases. It should be emphasized that a proper grouping does not lead to a decrease in remainder error tolerance bound. For instance, if we delete the 3rd group and only consider the 1st and 2nd groups in (24). Apparently, the remainder error tolerance bound in this case is

$$\frac{1}{4}\min\left\{\frac{f_{\text{Nyq}}}{PQ},\frac{f_{\text{Nyq}}}{PL}\right\}\equiv\frac{1}{4}\frac{f_{\text{Nyq}}}{PL}, \tag{32}$$

which indicates that the remainder error tolerance bound is invariable before and after grouping. Another advantage of this simplified grouping is to reduce computational complexity. However, the main drawback of such a grouping is the decrease in the number of groups, which may increase the risk of failure of the consistency criterion in practice. In a nutshell, 2-group or 3-group strategy is recommended. In practical use, a specific grouping strategy depends on the limitations of computational complexity and remainder errors.

5.3.2. Comparison to TDE

TDE is a classic frequency estimation method, which directly estimates the target frequency by (11). Because $0\leqslant\phi<2\pi$, it requires the delay between two cosets to be less than Nyquist interval, that is, the corresponding equivalent sampling frequency is required to reach Nyquist rate. However, the extremely small delay, i.e., high equivalent sampling frequency usually leads to unacceptable errors due to the presence of phase error; Thus, TDE is not practical in noisy environments. In contrast, the proposed method can significantly reduce interference of phase errors in frequency estimation. Let us assume the phase error due to noise is $\Delta\phi$[5]. It is not hard to derive the frequency estimation error caused by the phase error is $\frac{|\Delta\phi|}{2\pi}f_{\text{Nyq}}$. The remainder errors due to the phase error respectively are $\frac{|\Delta\phi|}{2\pi}\frac{f_{\text{Nyq}}}{P}$, $\frac{|\Delta\phi|}{2\pi}\frac{f_{\text{Nyq}}}{Q}$, and $\frac{|\Delta\phi|}{2\pi}\frac{f_{\text{Nyq}}}{L}$ from the three delay schemes. The final estimation error obtained by the proposed method is the average of the remainder errors, i.e., $\frac{1}{3}\frac{|\Delta\phi|}{2\pi}\left(\frac{f_{\text{Nyq}}}{P}+\frac{f_{\text{Nyq}}}{Q}+\frac{f_{\text{Nyq}}}{L}\right)$. Additionally, assuming the phase error conforms to a Gaussian distribution, we can obtain a lower error bound according to the error propagation formula,

$$\frac{1}{3}\sqrt{\frac{1}{P^2}+\frac{1}{Q^2}+\frac{1}{L^2}}\cdot\frac{|\Delta\phi|}{2\pi}f_{\text{Nyq}}\ll 1\cdot\frac{|\Delta\phi|}{2\pi}f_{\text{Nyq}}, \tag{33}$$

where $L\geqslant 3$ and $P\geqslant 1$. The sign $\ll$ is based on the inequality $\sqrt{\frac{1}{P^2}+\frac{1}{Q^2}+\frac{1}{L^2}}\leqslant\frac{1}{P}+\frac{1}{Q}+\frac{1}{L}\ll 3$.

Substituting the optimal configuration (30) into (33), the estimation error bound of the proposed method is

$$|\Delta f_t|\leqslant\begin{cases}\left(\frac{1}{L}+\frac{4}{3(L^3-L)}\right)\frac{|\Delta\phi|}{2\pi}f_{\text{Nyq}} & L\text{ is odd}\\ \left(\frac{1}{L}+\frac{16}{3(L^3-4L)}\right)\frac{|\Delta\phi|}{2\pi}f_{\text{Nyq}} & \gcd\{L,4\}=4\\ \left(\frac{1}{L}+\frac{64}{3(L^3-16L)}\right)\frac{|\Delta\phi|}{2\pi}f_{\text{Nyq}} & \gcd\{L,4\}=2\end{cases}, \tag{34}$$

where L needs to satisfy the constraint $L\leqslant\frac{1}{4}\frac{2\pi}{|\Delta\phi|}$ to ensure that (27) holds and thus the folding integers can be accurately determined. According to (34), it is recommended to use odd L in DCS to reduce the frequency estimation error.

[5]Phase error is equivalent to the remainder error up to a scaling factor, $|\Delta\tilde{r}_{ai}|=|\Delta\tilde{f}_{ai}|=\frac{|\Delta\phi|}{2\pi}\tilde{f}_{si}$.

6. Numerical Validation

In this section, we present some simulation results to validate the proposed methods for frequency identification from complex-valued and real-valued signals, respectively. First, a total of 4,200 samples are generated at a Nyquist rate of $f_{\text{Nyq}} = 1,050$ MHz. Then, the Nyquist samplers are downsampled by three sub-Nyquist sampling schemes, DCS ($P = 10, Q = 11$), CS ($U = 3, V = 7$), DCS ($P = 1, Q = 20$). The sub-Nyquist samples from DCS ($P = 10, Q = 11$) and DCS ($P = 1, Q = 20$) are respectively analyzed by the proposed method and TDE to identify frequencies. The CS samples are used to calculate the aliasing frequencies by DFT and estimate the true frequencies by solving the congruence equations. According to Theorem 1 and Theorem 3, the supremum frequency that can be identified is 1050 MHz and 525 MHz in the complex-valued and real-valued cases, respectively. Therefore, we randomly generate K frequency components with identical power, which are uniformly distributed in $[0, 1050)$ MHz and $[0, 525)$ HMz in the complex-valued and real-valued cases, respectively.

6.1. Single test result for demonstration

In this subsection, we present a single test result to demonstrate the effectiveness for multi-frequency case. Herein, $K = 2$ and SNR = 10 dB.

6.1.1. Complex-valued signals

The characteristic frequency is $\{f_1, f_2\} = \{678, 1012\}$ MHz. Firstly, we use AATDE to calculate $\tilde{f}_{si}$ and $\tilde{f}_{ai}$ from DCS ($P = 10, Q = 11$) samples. Fig. 6 presents the constructed delay schemes and the calculation of $\tilde{f}_{ai}$. In Fig. 6, the amplitude spectrum is the aliasing spectrum of sub-Nyquist samples ($f_s = 50$ MHz), which provides references for the phase locations. Once the phase locations are determined, phases are also determined and then the $\tilde{f}_{ai}$ are calculated by (11). Remarkably, the amplitude spectrum is almost constant in different delay schemes; thus, the multiple frequencies and their aliasing frequencies do clearly correspond. For example, the $\tilde{f}_{ai}(1)$ are the equivalent aliasing frequencies of a certain true frequency and $\tilde{f}_{ai}(2)$ represents the equivalent aliasing frequencies of another true frequency. Therefore, the multi-frequency estimation problem can be naturally simplified to multiple independent single frequency estimation problems, which can be solved efficiently.

Table 4: Results obtained by AATDE in the complex-valued case.

$\tilde{f}_{si}$ MHz	$\phi(1)$ rad	$\tilde{f}_{ai}(1)$ MHz	$\phi(2)$ rad	$\tilde{f}_{ai}(2)$ MHz
105	3.997	66.79	2.875	48.05
1050/11	3.795	57.65	0.643	9.77
50	1.509	12.01	3.517	27.99

We present the results from AATDE in Table 4. According to the equivalent sampling frequencies and

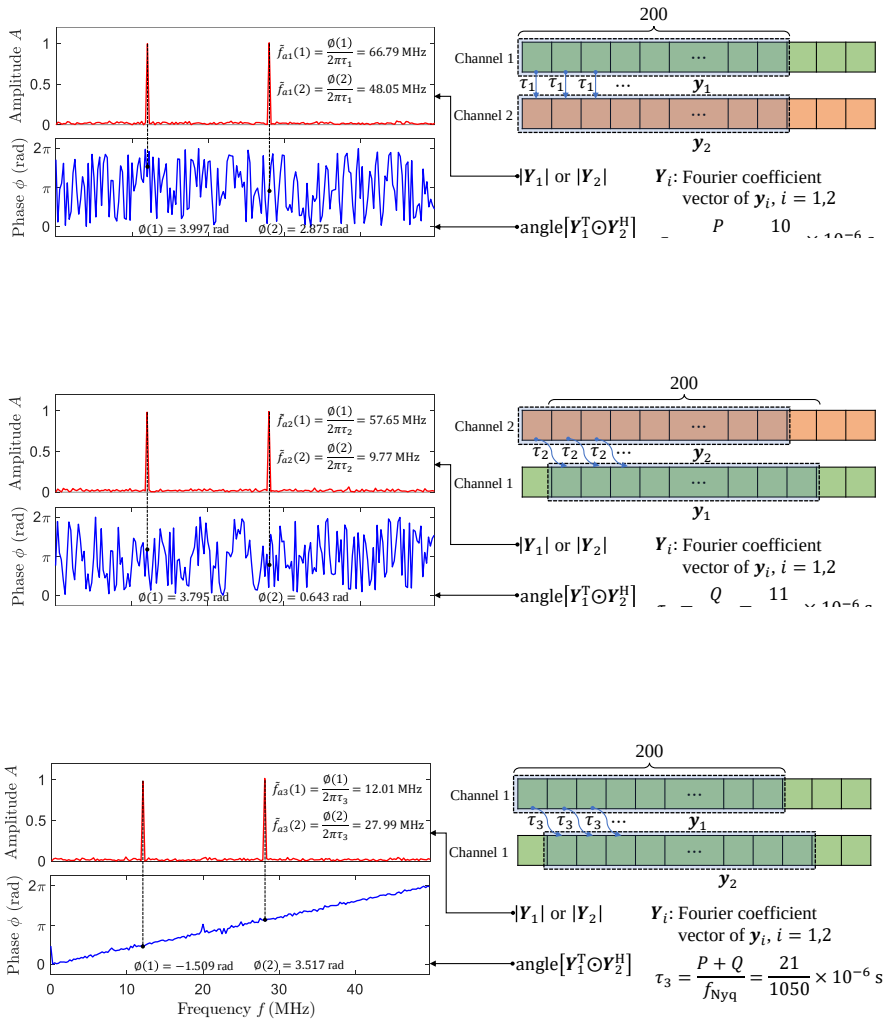

(c)

Figure 6: Calculation of the equivalent aliasing frequencies in the complex-valued case: (a) the 1st, (b) the 2nd, and (c) the 3rd delay schemes.

aliasing frequencies in Table 4, we have two congruence equations,

$$\begin{cases} \mathrm{mod}(f_1, 105) = 66.79 \\ \mathrm{mod}(f_1, \dfrac{1050}{11}) = 57.65 \\ \mathrm{mod}(f_1, 50) = 12.01 \end{cases} ; \quad \begin{cases} \mathrm{mod}(f_2, 105) = 48.05 \\ \mathrm{mod}(f_2, \dfrac{1050}{11}) = 9.77 \\ \mathrm{mod}(f_2, 50) = 27.99 \end{cases} .$$

By solving the two congruence equations using CR-CRT, we obtain the estimates of f_1 and f_2, i.e., $\hat{f}_1 = 1011.998$ HMz and $\hat{f}_2 = 677.997$ HMz, which are very close to the true values ($f_1 = 1012$ MHz, $f_2 = 678$ MHz).

6.1.2. Real-valued signals

Furthermore, we set out to demonstrate the effectiveness of the proposed method for real-valued signals. Here, $\{f_1, f_2\} = \{339, 506\}$ MHz. Similarly, the constructed delay schemes and the calculation of $\tilde{f}_{ai}$ are presented in Fig. 7. Different from the complex-valued case, there are four peaks in the aliasing amplitude spectrum, which are symmetrically distributed in the 1st and 2nd Nyquist zones, respectively. According to the law of periodic extension, the peaks in $[0, 25)$ and $[25, 50)$ MHz are the aliasing result of true frequencies and its

negative duplicates. However, the correspondence is ambiguous. In this case, we map the phase to range $(-\pi, \pi]$ to calculate $\tilde{f}_{ai}$. The phases in $[0, 25)$ and $[25, 50)$ MHz are opposite; thus, we only consider the peaks and phases in the 1st Nyquist zone. The equivalent sampling frequencies and aliasing frequencies obtained by AATDE are summarized in Table 5. Notably, $\tilde{f}_{ai}$ obtained by (18) is numerically equal to $\min_{\kappa \in \mathbb{N}} |f_t - \kappa \tilde{f}_{si}|$, which leads to the ambiguity between (equivalent) aliasing frequencies and remainders as shown in (23). To eliminate this ambiguity, we use GSCR-CRT to reconstruct true frequencies individually and the reconstruction results of f_2 are presented in Table 6. By the consistency criterion, we can locate combinations 4 and 5. Furthermore, by the minimum estimation criterion, case 5 is considered confident. Thus, $\hat{f}_2 = (505.99 + 506.01 + 505.97)/3 = 505.99$ MHz and its error is only 0.01 MHz. The high accuracy shows the effectiveness of the proposed method for real-valued signals with multiple frequencies.

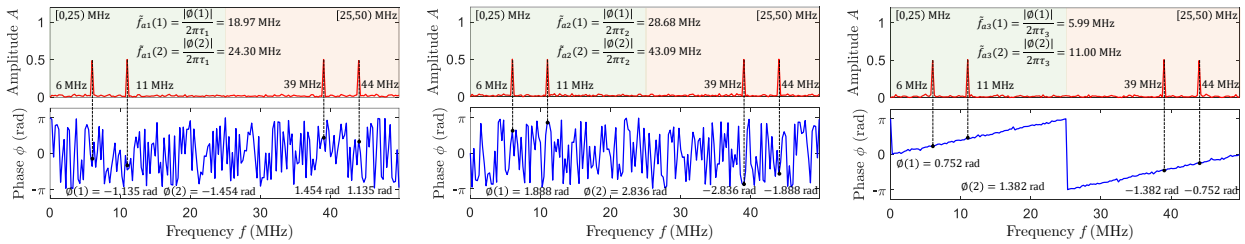

(a) (b) (c)

Figure 7: An example of ambiguity between the equivalent aliasing frequency and remainder in the real-valued case: (a) the 1st, (b) the 2nd, and (c) the 3rd delay schemes.

Table 5: The results obtained by AATDE in the real-valued case.

$\tilde{f}_{si}$ MHz	$\phi(1)$ rad	$\tilde{f}_{ai}(1)$ MHz	$\phi(2)$ rad	$\tilde{f}_{ai}(2)$ MHz
105	-1.135	18.97	-1.454	24.30
1050/11	1.888	28.68	2.836	43.09
50	0.752	5.99	1.382	11.00

Table 6: Reconstruction results of a single frequency.

No.	$\tilde{r}_{a1}$	$\tilde{r}_{a2}$	$\tilde{r}_{a3}$	$\tilde{f}_{s1}$	$\tilde{f}_{s2}$	$\tilde{f}_{s3}$
1	18.97	28.68	5.99	124.05	754.98	505.97
2	18.97	28.68	44.01	124.05	543.99	793.16
3	18.97	66.77	5.99	544.01	754.98	256.84
4	18.97	66.77	44.01	544.01	543.99	544.03
5	86.03	28.68	5.99	505.99	506.01	505.97
6	86.03	28.68	44.01	505.99	295.02	793.16
7	86.03	66.77	5.99	925.95	506.01	256.84
8	86.03	66.77	44.01	925.95	295.02	544.03

6.2. RMSE versus SNR

In this subsection, we present the statistical performance of the proposed method through 200 random tests where K frequencies are uniformly distributed. The statistical performance is evaluated by the root mean square error (RMSE) of the frequency estimation, defined as follows

$$\mathrm{RMSE}(f) = \sqrt{\frac{1}{200K}\sum_{r=1}^{200}\sum_{k=1}^{K}\left(\hat{f}_k(r) - f_k\right)^2}, \tag{35}$$

where $\hat{f}_k(r)$ is the estimate of f_k from the rth random trial.

To further verify its effectiveness, the proposed method is compared with several representative frequency estimation methods including CR-CRT [18], Candan [1, 2], TDE [33, 34], MUSIC [37, 38], and Periodogram [39, 40]. For a fair comparison, the frequency resolution of Candan, MUSIC, and Periodogram are set to the same as the proposed method in the active aliasing stage ($50/200 = 0.25$ Hz).

6.2.1. Complex-valued signals

The RMSE results in the complex-valued case are presented in Fig. 8(a), where single frequency ($K = 1$) and multi-frequency case ($K = 5$) are both considered. Sub-Nyquist sampling schemes, DCS ($P = 10, Q = 11$), CS ($U = 3, V = 7$), DCS ($P = 1, Q = 20$) are respectively used in the proposed method, CR-CRT, and TDE, and their average sampling rates are 100, 500, and 100 MHz. The rest methods employ the same sampling schemes as the proposed method for a fair comparison. The proposed method and CR-CRT require aliasing information which are respectively obtained by AATDE and DFT. Remarkably, in the case of $-10 \leqslant \mathrm{SNR} \leqslant 30$ dB, the frequency peaks in the DFT spectra are clear and the aliasing frequencies are the same for different SNRs. Therefore, the RMSE of frequency estimations obtained by CR-CRT is constant in the simulation. Furthermore, DFT suffers from frequency resolutions and thus these exists errors in frequency estimations from CR-CRT. From Fig. 8(a), RMSE of the proposed method is obviously lower than that of TDE, which validates the effectiveness of the proposed method in terms of reducing estimation error. Furthermore, the proposed method outperforms CR-CRT, MUSIC, and the Periodogram, particularly at high SNRs, owing to the gridless nature of AATDE. In contrast, since Candan's method is not applicable to sub-Nyquist sampling, it exhibits unsatisfactory performance. Then, we compare the results of single frequency and multi-frequency cases. It should be emphasized that the CR-CRT is not applicable to multi-frequency cases due to the ambiguity between multiple frequencies and their aliasing frequencies. The proposed method is still effective for the multi-frequency case in the high SNR case even though its performance is slightly degraded compared with that in single frequency cases. In the multi-frequency cases, the mutual coupling between frequencies in the aliasing spectrum causes additional phase error, which is the main cause of the performance degradation.

6.2.2. Real-valued signals

Fig. 8(b) shows the RMSE of frequency estimation in the real-valued case. Due to the ambiguity between aliasing frequencies and remainders, CR-CRT is not applicable to the real-valued case, and we add a two opposite numbers-based CRT (TON-CRT) [41, 42] for comparison. Note that, TON-CRT is only applicable to

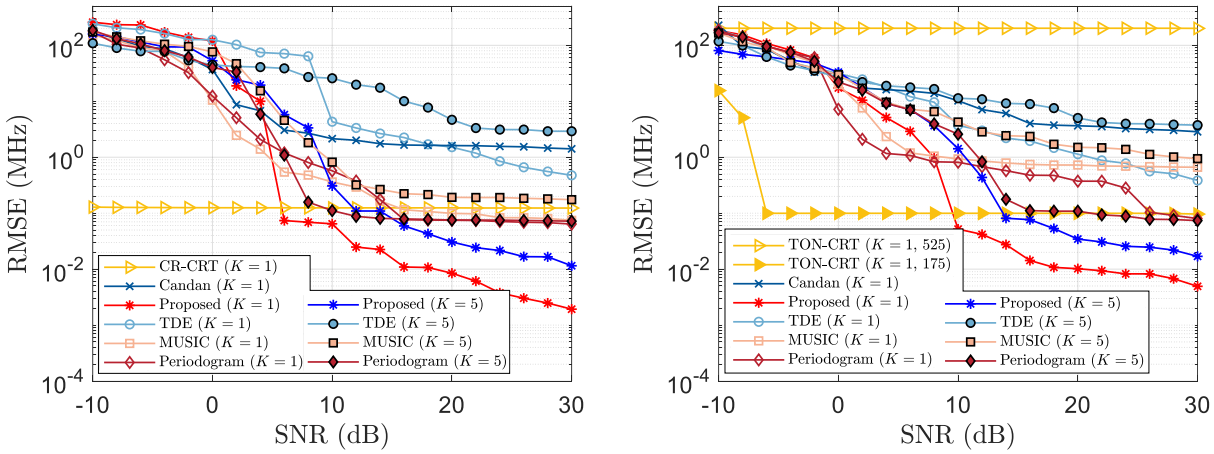

(a) (b)

Figure 8: RMSE versus SNR in the (a) complex-valued case and (b) real-valued case.

real-valued single-frequency single in coprime sampling and it can only identify the frequency up to 175 MHz with CS (150 MHz and 350 MHz); thus, it cannot work when the characteristic frequency is set to [0, 525) MHz, as shown in the RMSE marked 525. Fig. 8(b) indicates the proposed method can be applied to real-valued signals and its estimation accuracy of the proposed method is significantly higher than those of Candan, TDE, MUSIC and Periodogram. Furthermore, it should be emphasized that almost all existing CRT-based frequency estimation algorithms are limited by their poor applicability. Fortunately, the proposed method has superior applicability to complex-valued and real-valued signals, single-frequency and multi-frequency cases.

7. Conclusion

This paper has proposed a novel CRT-based frequency estimation method that reduces the required sampling rate and simplifies hardware configurations. Significantly, it is applicable to real-valued waveforms as well as in multiple-frequency cases. In terms of structure, the proposed method only requires a special periodic nonuniform sampling of order 2, which is simpler than multi-rate sampling. In terms of mining aliasing information, the proposed method equivalently generates aliasing information by phase change caused by delay and estimates frequencies by solving the congruence equations constructed by the aliasing findings. Owing to the clear correspondence between the multiple frequencies and their aliasing frequencies, the proposed method can be applied to multiple-frequency estimation. Furthermore, the proposed method can be extended to real-valued waveforms by incorporating grouping operations and frequency estimation sifting. Owing to its high practicality, the proposed method has potential applications in communications, measurements, and radar detection.

In summary, the paper overcomes the main limitations of CRT in frequency estimation of undersampled waveforms without additional hardware configuration and unacceptable computational complexity, and thus is expected to lead to a renaissance of CRT in undersampled signal processing.

However, we have to admit that the proposed method cannot work at extremely low SNRs due to the phase-based aliasing frequency calculation. In the future, new aliasing frequency estimation techniques to improve the

robustness to severe noise are worth studying.

Appendix A: Proof of Theorem 1

Proof. By definition, $\tilde{f}_{si} \triangleq 1/\tau_i$. Any achievable delay in DCS can be expressed by a linear combination of PT and LT with integer coefficients. Thus, we have $\{\tilde{f}_{s1}, \tilde{f}_{s2}, \tilde{f}_{s3}, \cdots, \tilde{f}_{sS}\} = \{\frac{f_{\text{Nyq}}}{P}, \frac{f_{\text{Nyq}}}{Q}, \frac{f_{\text{Nyq}}}{L}, \cdots, \frac{f_{\text{Nyq}}}{mP+nL}\}$ where $m \in \{-1, 0, 1\}$ and $n \in \mathbb{N}$. Because $\gcd\{L, P\} = \gcd\{L, Q\} = \gcd\{P, Q\} = 1$, $\text{glcm}\{\tilde{f}_{s1}, \tilde{f}_{s2}, \cdots, \tilde{f}_{sS}\} = f_{\text{Nyq}}$ for any integer $S \geqslant 2$. From Corollary 1, $f_{\text{sup}} = f_{\text{Nyq}}$, Q.E.D.

Appendix B: Proof of Theorem 2

The proof is divided into two parts: sufficiency and necessity.

Sufficiency proof [23]. $\hat{q}_{i1} = \left[\frac{(\tilde{f}_{ai} - \tilde{f}_{a1})}{m_{1i}}\right]$ where $m_{1i} \triangleq \text{ggcd}\{\tilde{f}_{s1}, \tilde{f}_{si}\}$ and $[\cdot]$ denotes rounding operation; thus, $\hat{q}_{i1} = \left[\frac{(\tilde{f}^*_{ai} + \Delta\tilde{f}_{ai} - \tilde{f}^*_{a1} - \Delta\tilde{f}_{a1})}{\text{ggcd}\{\tilde{f}_{s1}, \tilde{f}_{si}\}}\right] = q_{i1} + \left[\frac{(\Delta\tilde{f}_{ai} - \Delta\tilde{f}_{a1})}{\text{ggcd}\{\tilde{f}_{s1}, \tilde{f}_{si}\}}\right]$ where $\hat{q}_{i1}$ is an estimate of q_{i1} in the presence of remainder errors. Since $|\Delta\tilde{f}_{ai} - \Delta\tilde{f}_{a1}| \leqslant \text{ggcd}\{\tilde{f}_{s1}, \tilde{f}_{si}\}/2$, $\left[\frac{(\Delta\tilde{f}_{ai} - \Delta\tilde{f}_{a1})}{\text{ggcd}\{\tilde{f}_{s1}, \tilde{f}_{si}\}}\right] = 0$ and $\hat{q}_{i1} = q_{i1}$. In this case, $\hat{\xi}_{i1}$ can be accurately calculated by $\text{mod}(\hat{q}_{i1}\bar{\Gamma}_i, \Gamma_{i1})$, i.e., $\hat{\xi}_{i1} = \xi_{i1}$ where $\xi_{i1} \triangleq \text{mod}(q_{i1}\bar{\Gamma}_i, \Gamma_{i1})$. Thus, $\hat{\xi}_{i1} = \text{mod}(\hat{\text{n}}_1, \Gamma_{\text{i1}})$ can be equivalently written as $\xi_{i1} = \text{mod}(\text{n}_1, \Gamma_{\text{i1}})$. That is, the $\hat{n}_1$ obtained by solving the congruence equations $\hat{\xi}_{i1} = \text{mod}(\hat{n}_1, \Gamma_{i1})$ is equal to the true folding integer, i.e., $n_1 = \hat{n}_1$. From $n_1\tilde{f}_{s1} \leqslant f_t \leqslant \text{glcm}\{\tilde{f}_{s1}, \tilde{f}_{s2}, \cdots, \tilde{f}_{sS}\}$, we have $n_1 \leqslant \text{lcm}\{\Gamma_{21}, \Gamma_{31}, \cdots, \Gamma_{S1}\}$. Thus, according to CR-CRT, n_1 can be uniquely reconstructed by solving the above congruence equations. After n_1 is determined, we can calculate other integers n_i for $2 \leqslant i \leqslant S$ from **Algorithm 2**. Therefore, $\hat{n}_i = n_i$ for $2 \leqslant i \leqslant S$. Hence the above analysis proves the sufficiency.

Necessity proof [23]. Assume that there exists one remainder error that contradicts (15). Without loss of generality, assume the exception is the jth remainder, i.e., $|\Delta\tilde{f}_{aj} - \Delta\tilde{f}_{a1}| > \text{ggcd}\{\tilde{f}_{s1}, \tilde{f}_{sj}\}/2$. It follows that $\left[\frac{(\Delta\tilde{f}_{aj} - \Delta\tilde{f}_{a1})}{\text{ggcd}\{\tilde{f}_{s1}, \tilde{f}_{sj}\}}\right] \neq 0$ and $\hat{q}_{j1} \neq q_{j1}$. We have the following two cases.

Case 1): Γ_{j1} is a divisor of $[(\Delta\tilde{f}_{aj} - \Delta\tilde{f}_{a1})/\text{ggcd}\{\tilde{f}_{s1}, \tilde{f}_{sj}\}]$, it follows that $\hat{\xi}_{j1} = \text{mod}(\hat{q}_{j1}\bar{\Gamma}_j, \Gamma_{j1}) = \text{mod}(q_{j1}\bar{\Gamma}_j, \Gamma_{j1}) = \xi_{j1}$. Hence, from **Algorithm 2**, n_1 can be correctly reconstructed, i.e., $\hat{n}_1 = n_1$.

Case 2): Γ_{j1} is not a divisor of $[(\Delta\tilde{f}_{aj} - \Delta\tilde{f}_{a1})/\text{ggcd}\{\tilde{f}_{s1}, \tilde{f}_{sj}\}]$. Assuming $\hat{\xi}_{j1} = \xi_{j1}$, we have $\exists k \in \mathbb{Z}$, $\hat{q}_{j1}\bar{\Gamma}_j - q_{j1}\bar{\Gamma}_j = k\Gamma_{j1}$. Multiplying this equation by Γ_{1j} and considering $\bar{\Gamma}_j\Gamma_{1j} = 1 + k\Gamma_{j1}$ for some $k \in \mathbb{Z}$, we have $\hat{q}_{j1} - q_{j1} = k\Gamma_{j1}$ for some $k \in \mathbb{Z}$. By definition, $\hat{q}_{j1} \triangleq [(\tilde{f}_{aj} - \tilde{f}_{a1})/m_{1j}] = [(\tilde{f}^*_{aj} + \Delta\tilde{f}_{aj} - \tilde{f}^*_{a1} - \Delta\tilde{f}_{a1})/\text{ggcd}\{\tilde{f}_{s1}, \tilde{f}_{sj}\}] = q_{j1} + [(\Delta\tilde{f}_{aj} - \Delta\tilde{f}_{a1})/\text{ggcd}\{\tilde{f}_{s1}, \tilde{f}_{sj}\}]$. Thus, $[(\Delta\tilde{f}_{aj} - \Delta\tilde{f}_{a1})/\text{ggcd}\{\tilde{f}_{s1}, \tilde{f}_{sj}\}] = k\Gamma_{j1}$, which contradicts with the premise. Thus, the assumption is not valid. Since $\hat{\xi}_{j1} \neq \xi_{j1}$, n_1 and $\hat{n}_1$ have different congruences. Thus, $\hat{n}_1 \neq n_1$. Apparently, from (14), we have $\hat{n}_j \neq n_j$.

From **Case 1)** and **Case 2)**, if condition (15) is not satisfied, the folding number n_i cannot be accurately determined. This proves the necessity. Q.E.D.

Appendix C: Proof of Corollary 2

Proof. In DCS, using the first equation as the reference to differentiate can maximize the error tolerance bound. Thus, we have

$$\max_{1\leqslant k\leqslant S}\min_{1\leqslant j\neq k\leqslant S}\frac{\text{ggcd}\{\tilde{f}_{sk},\tilde{f}_{sj}\}}{4}=\min_{1\leqslant j\neq k\leqslant S}\frac{\text{ggcd}\{\tilde{f}_{s1},\tilde{f}_{sj}\}}{4},$$

Apparently, if $|\Delta\tilde{f}_{ai}|<\min_{1\leqslant j\neq k\leqslant S}\text{ggcd}\{\tilde{f}_{s1},\tilde{f}_{sj}\}/4$, it follows that $|\Delta\tilde{f}_{ai}-\Delta\tilde{f}_{a1}|\leqslant\text{ggcd}\{\tilde{f}_{s1},\tilde{f}_{si}\}/2$. Therefore, (16) is the sufficient condition for (15). By Theorem 2, n_i can be accurately determined. Q.E.D.

Appendix D: Proof of Theorem 3

Proof. In this proof, we do not consider the reconstruction failure due to the remainder errors, i.e., the folding integers can be accurately determined by CR-CRT. It is not hard to find if Theorem 3 is proven to be true in the absence of reconstruction failure, the target frequency f_t can be uniquely identified in the presence of remainder errors as long as $f_t\leqslant f_{\text{sup}}$ and the remainder errors satisfy (16). Let us continue to prove.

According to the definitions of $\tilde{f}_{s1}$,$\tilde{f}_{s2}$,$\tilde{f}_{s3}$ given in Section 3.2, we have $\text{glcm}\{\tilde{f}_{s1},\tilde{f}_{s2}\}=\text{glcm}\{\tilde{f}_{s1},\tilde{f}_{s3}\}=\text{glcm}\{\tilde{f}_{s2},\tilde{f}_{s3}\}=f_{\text{Nyq}}$. Therefore, by CR-CRT, the target frequency f_t can be reconstructed if $f_t<f_{\text{Nyq}}$ and the remainders are correctly selected. Assume the correct remainders of f_t modulo $\tilde{f}_{s1}$, $\tilde{f}_{s2}$, and $\tilde{f}_{s3}$ are r^*_{a1}, r^*_{a2} and r^*_{a3}, respectively, particularly, $r^*_{ai}\in\{\tilde{r}_{ai},\tilde{f}_{si}-\tilde{r}_{ai}\}$ for each $1\leqslant i\leqslant 3$. On the premise of $0\leqslant f_t<f_{\text{Nyq}}$ and the all remainders are correctly selected, f_t can be successfully reconstructed from each group; and the corresponding reconstruction results are $(n_1\tilde{f}_{s1}+\tilde{r}^*_{a1}+n_2\tilde{f}_{s2}+\tilde{r}^*_{a2})/2$, $(n_1\tilde{f}_{s1}+\tilde{r}^*_{a1}+n_3\tilde{f}_{s3}+\tilde{r}^*_{a3})/2$, and $(n_2\tilde{f}_{s2}+\tilde{r}^*_{a2}+n_3\tilde{f}_{s3}+\tilde{r}^*_{a3})/2$, where $n_i=\lfloor f_t/\tilde{f}_{si}\rfloor$ for each $1\leqslant i\leqslant 3$.

Then, we consider the opposite case where each remainder is mistakenly selected. The true remainders are r^*_{a1}, r^*_{a2} and r^*_{a3}; however, we mistakenly consider $\tilde{f}_{s1}-r^*_{a1}$, $\tilde{f}_{s2}-r^*_{a2}$, and $\tilde{f}_{s3}-r^*_{a3}$ as the remainders for congruence equations. In this case, $\tilde{f}_{s1}-r^*_{a1}$, $\tilde{f}_{s2}-r^*_{a2}$, and $\tilde{f}_{s3}-r^*_{a3}$ are actually are the remainders of $f_{\text{Nyq}}-f_t$ modulo $\tilde{f}_{s1}$, $\tilde{f}_{s2}$, and $\tilde{f}_{s3}$ because $\text{mod}(f_{\text{Nyq}},\tilde{f}_{si})=0$ for $1\leqslant i\leqslant 3$. Therefore, if $0\leqslant f_t<f_{\text{Nyq}}$ and each remainder is mistakenly selected, the corresponding reconstruction results actually are estimates of $f_{\text{Nyq}}-f_t$, and the specific results are $(z_1\tilde{f}_{s1}-\tilde{r}^*_{a1}+z_2\tilde{f}_{s2}-\tilde{r}^*_{a2})/2$, $(z_1\tilde{f}_{s1}-\tilde{r}^*_{a1}+z_3\tilde{f}_{s3}-\tilde{r}^*_{a3})/2$, and $(z_2\tilde{f}_{s2}-\tilde{r}^*_{a2}+z_3\tilde{f}_{s3}-\tilde{r}^*_{a3})/2$, where $z_i=\lfloor(f_{\text{Nyq}}-f_t)/\tilde{f}_{si}\rfloor+1=(f_{\text{Nyq}}/\tilde{f}_{si})-n_i$. In this case, the variance of frequency estimations is the same as the previous once. Therefore, the consistency criterion cannot uniquely determine the valid frequency estimation from those two cases. To completely separate these two cases, a sufficient and necessary conditions is $0\leqslant f_t\leqslant f_{\text{Nyq}}/2$. On the premise of $0\leqslant f_t\leqslant f_{\text{Nyq}}/2$, $f_t\leqslant f_{\text{Nyq}}-f_t$. Hence, we can always uniquely determine valid frequency estimation by **consistency criterion** and **minimum estimation criterion**[6]. Q.E.D.

[6]The minimum average of the estimations from the two sets of estimations with the minimum variance is regarded as the final estimation

Appendix E: Proof of Corollary 3

Proof. According to Theorem 2, when the remainder errors satisfy (E1), the folding integers n_i can be correctly reconstructed from (24).

$$\begin{cases} \left|\Delta\tilde{f}_{a2}-\Delta\tilde{f}_{a1}\right| \leqslant \frac{1}{2}\mathrm{ggcd}\left\{\tilde{f}_{s1},\tilde{f}_{s2}\right\} = \frac{1}{2}\frac{f_{\mathrm{Nyq}}}{PQ} \\ \left|\Delta\tilde{f}_{a3}-\Delta\tilde{f}_{a1}\right| \leqslant \frac{1}{2}\mathrm{ggcd}\left\{\tilde{f}_{s1},\tilde{f}_{s3}\right\} = \frac{1}{2}\frac{f_{\mathrm{Nyq}}}{PL} \\ \left|\Delta\tilde{f}_{a3}-\Delta\tilde{f}_{a2}\right| \leqslant \frac{1}{2}\mathrm{ggcd}\left\{\tilde{f}_{s2},\tilde{f}_{s3}\right\} = \frac{1}{2}\frac{f_{\mathrm{Nyq}}}{QL} \end{cases}. \tag{E1}$$

Eq. (27) is a simpler sufficient condition for (E1). Obviously, if $\Delta\tilde{f}_{ai}$ satisfies (27), (E1)) hold true and then n_i can be correctly reconstructed.

Moreover, according to Theorem 3, f_t can be uniquely and effectively estimated from each congruence equation group (24) in the case of $f_t \in [0, f_{\mathrm{Nyq}}/2]$ and the corresponding results are $(n_1\tilde{f}_{s1}+\tilde{r}_{a1}+n_2\tilde{f}_{s2}+\tilde{r}_{a2})/2$, $(n_1\tilde{f}_{s1}+\tilde{r}_{a1}+n_3\tilde{f}_{s3}+\tilde{r}_{a3})/2$, and $(n_2\tilde{f}_{s2}+\tilde{r}_{a2}+n_3\tilde{f}_{s3}+\tilde{r}_{a3})/2$, respectively. The final estimate is their mean, i.e., $\hat{f}_t = (n_1\tilde{f}_{s1}+\tilde{r}_{a1}+n_2\tilde{f}_{s2}+\tilde{r}_{a2}+n_3\tilde{f}_{s3}+\tilde{r}_{a3})/3$. Because n_1, n_2, n_3 are correct, we only need to consider the impact of remainder errors on the final estimate. According to the error propagation formula, we have

$$|\Delta\hat{f}_t| = \sqrt{\Delta\tilde{f}_{a1}^2+\Delta\tilde{f}_{a2}^2+\Delta\tilde{f}_{a3}^2}/3, \tag{E2}$$

where $\Delta\hat{f}_t$ denotes the estimation error of $\hat{f}_t$.

Substituting (27) into (E2), we have the inequality

$$|\Delta\hat{f}_t| < \frac{\sqrt{3}}{12}\min\left\{\frac{f_{\mathrm{Nyq}}}{PQ},\frac{f_{\mathrm{Nyq}}}{PL},\frac{f_{\mathrm{Nyq}}}{QL}\right\}, \tag{E3}$$

therefore, this proves Corollary 3. Q.E.D.

8. Acknowledgement

Thanks to Xiang-Gen Xia and his coauthors for their profound works in robust CRT. This work was supported by the National Natural Science Foundation of China (Nos. 523B2044, 52222504, and 92360306). The work of Asoke K. Nandi was supported in part by the Royal Society Award (No. IEC\NSFC\223294).

References

[1] C. Candan, A method for fine resolution frequency estimation from three DFT samples, IEEE Signal Process. Lett. 18 (2011) 351–354.

[2] Ç. Candan, Fine resolution frequency estimation from three DFT samples: Case of windowed data, Signal Process. 114 (2015) 245–250.

[3] L. Xiao, X.-G. Xia, Frequency determination from truly sub-nyquist samplers based on robust chinese remainder theorem, Signal Process. 150 (2018) 248–258.

[4] J. Cao, Z. Yang, R. Sun, X. Chen, Delay sampling theorem: A criterion for the recovery of multitone signal, Mech. Syst. Signal Process. 200 (2023) 110523.

[5] L. Marple, A new autoregressive spectrum analysis algorithm, IEEE Trans. Acoustics, Speech, and Signal Process. 28 (1980) 441–454.

[6] D. Potts, M. Tasche, Parameter estimation for exponential sums by approximate prony method, Signal Process. 90 (2010) 1631–1642.

[7] S. Kay, S. Saha, Mean likelihood frequency estimation, IEEE Trans. Signal Process. 48 (2000) 1937–1946.

[8] H. Fu, P. Y. Kam, MAP/ML estimation of the frequency and phase of a single sinusoid in noise, IEEE Trans. Signal Process. 55 (2007) 834–845.

[9] H. C. So, F. K. W. Chan, W. Sun, Subspace approach for fast and accurate single-tone frequency estimation, IEEE Trans. Signal Process. 59 (2010) 827–831.

[10] J. Cao, Z. Yang, H. Li, G. Teng, S. Tian, W. Li, X. Chen, Rotating blade frequency identification by single-probe blade tip timing, Mech. Systems Signal Process. 172 (2022) 108961.

[11] J. Cao, R. Sun, L. Lu, Z. Yang, X. Chen, Blind power spectrum reconstruction for multi-sinusoid signals with generative multicoset sampling, Signal Process. 226 (2025) 109644.

[12] Z. Yang, J. Tang, Y. C. Eldar, L. Xie, On the sample complexity of multichannel frequency estimation via convex optimization, IEEE Trans. Inf. Theory 65 (2018) 2302–2315.

[13] H. Ahmed, A. K. Nandi, Compressive sampling and feature ranking framework for bearing fault classification with vibration signals, IEEE Access 6 (2018) 44731–44746.

[14] L. Liu, J.-F. Gu, P. Wei, Joint doa and frequency estimation with sub-nyquist sampling, Signal Process. 154 (2019) 87–96.

[15] J. Cao, Z. Yang, X. Zhang, X. Chen, Compressed covariance sensing for blade tip timing measurement, J. Sound Vib. 579 (2024) 118376.

[16] H. Nyquist, Certain topics in telegraph transmission theory, Transactions of the American Institute of Electrical Engineers 47 (1928) 617–644.

[17] C. E. Shannon, Communication in the presence of noise, Proceedings of the IRE 37 (1949) 10–21.

[18] W. Wang, X.-G. Xia, A closed-form robust Chinese remainder theorem and its performance analysis, IEEE Trans. Signal Process. 58 (2010) 5655–5666.

[19] X.-G. Xia, G. Wang, Phase unwrapping and a robust chinese remainder theorem, IEEE Signal Process. Lett. 14 (2007) 247–250.

[20] X. Li, X.-G. Xia, A fast robust chinese remainder theorem based phase unwrapping algorithm, IEEE Signal Process. Lett. 15 (2008) 665–668.

[21] X. Li, H. Liang, X.-G. Xia, A robust chinese remainder theorem with its applications in frequency estimation from undersampled waveforms, IEEE Trans. Signal Process. 57 (2009) 4314–4322.

[22] W. Wang, X. Li, W. Wang, X.-G. Xia, Maximum likelihood estimation based robust chinese remainder theorem for real numbers and its fast algorithm, IEEE Trans. Signal Process. 63 (2015) 3317–3331.

[23] L. Xiao, X.-G. Xia, W. Wang, Multi-stage robust chinese remainder theorem, IEEE Trans. Signal Process. 62 (2014) 4772–4785.

[24] X. Li, X.-G. Xia, W. Wang, W. Wang, A robust generalized chinese remainder theorem for two integers, IEEE Trans. Inf. Theory 62 (2016) 7491–7504.

[25] H. Xiao, G. Xiao, Notes on crt-based robust frequency estimation, Signal Process. 133 (2017) 13–17.

[26] H. Xiao, Y. Huang, Y. Ye, G. Xiao, Robustness in chinese remainder theorem for multiple numbers and remainder coding, IEEE Trans. Signal Process. 66 (2018) 4347–4361.

[27] H. Xiao, Y. Zhang, B. Zhou, G. Xiao, On the foundation of sparsity constrained sensing (part i): Necessary and sufficient sampling theory and robust remainder problem, IEEE Trans. Signal Process. 71 (2023) 1263–1276.

[28] X. Huang, H. Wang, H. Qin, W. Nie, Frequency estimator based on spectrum correction and remainder sifting for undersampled real-valued waveforms, IEEE Access 7 (2019) 25980–25988.

[29] Y. C. Eldar, Sampling theory: Beyond bandlimited systems, Cambridge University Press, 2015.

[30] J. H. McClellen, C. M. Rader, Number theory in digital Signal Process., Prentice Hall Professional Technical Reference, 1979.

[31] C. Luo, Non-uniform sampling: algorithms and architectures, Ph.D. thesis, Georgia Institute of Technology, 2012.

[32] J. Cao, Z. Yang, X. Chen, Delay coprime sampling: A simplified sub-nyquist sampling for noisy multi-sinusoidal signals, IEEE Signal Process. Lett. 31 (2024) 1720–1724.

[33] A. Piersol, Time delay estimation using phase data, IEEE Trans. Acoustics, Speech, and Signal Process. 29 (1981) 471–477.

[34] J. Cao, Z. Yang, S. Tian, H. Li, R. Jin, R. Yan, X. Chen, Biprobes blade tip timing method for frequency identification based on active aliasing time-delay estimation and dealiasing, IEEE Trans. Ind. Electron. 70 (2022) 1939–1948.

[35] J. Cao, Z. Yang, M. Lu, L. Lu, X. Chen, Active aliasing esprit: A robust parameter estimation method for low-intervention blade tip timing measurement, Mech. Syst. Signal Process. 227 (2025) 112392.

[36] J. Cao, Z. Yang, S. Tian, G. Teng, X. Chen, Active aliasing technique and risk versus error mechanism in blade tip timing, Mech. Syst. Signal Process. 191 (2023) 110150.

[37] R. Schmidt, Multiple emitter location and signal parameter estimation, IEEE Trans. Antennas Propag. 34 (1986) 276–280.

[38] J. Cao, Z. Yang, X. Chen, R. Yan, From pseudo to real: Generalized subspace method for power spectrum reconstruction, IEEE Trans. Ind. Electron. 71 (2023) 4141–4150.

[39] D. Rife, R. Boorstyn, Single tone parameter estimation from discrete-time observations, IEEE Trans. Inf. Theory 20 (2003) 591–598.

[40] P. Stoica, J. Li, H. He, Spectral analysis of nonuniformly sampled data: A new approach versus the periodogram, IEEE Trans. Signal Process. 57 (2008) 843–858.

[41] Y.-W. Zhang, X.-F. Han, G.-Q. Xiao, An efficient crt based algorithm for frequency determination from undersampled real waveform, Sensors 23 (2023) 452.

[42] J. Cao, Z. Yang, R. Sun, X. Chen, From theory to practice: Chinese remainder theorem-based blade tip timing measurement, IEEE Trans. Instrum. Meas. 74 (2025).